

# The nature of the optical—radio correlations for powerful radio galaxies

C.N. Tadhunter<sup>1</sup>, R. Morganti<sup>2,3</sup>, A. Robinson<sup>4</sup>, R. Dickson<sup>1</sup>, M. Villar-Martin<sup>1</sup>  
& R.A.E. Fosbury<sup>5</sup>

<sup>1</sup> Department of Physics, University of Sheffield, Sheffield S3 7RH

<sup>2</sup> Australia Telescope National Facility, CSIRO, PO Box 76, Epping, NSW2121, Australia

<sup>3</sup> Istituto di Radioastronomia, CNR, via Gobetti 101, I-40129 Bologna, Italy

<sup>4</sup> Division of Physical Sciences, University of Hertfordshire, College Lane, Hatfield, Herts AL10 9AB

<sup>5</sup> ST-ECF, European Southern Observatory, Karl-Schwarzschild-Strasse 2, D85748 Garching bei Munchen, Germany

**Abstract** The nature of the optical–radio correlations for powerful radio galaxies is investigated using spectroscopic observations of a complete sample of southern 2Jy radio sources. In line with previous work, we find that significant correlations exist between the luminosities of the [OIII] $\lambda$ 5007, [OII] $\lambda$ 3727 and H $\beta$  emission lines and the radio luminosity. However, our observations are not easily reconciled with the idea that these correlations are caused by the increase in the power of the photoionizing quasar as the jet power increases, with average ISM properties not changing appreciably with redshift or radio power: not only do we find that the scatter in the  $L_{\text{[OIII]}}$  vs.  $L_{\text{radio}}$  correlation is significantly larger than in  $L_{\text{[OII]}}$  vs.  $L_{\text{radio}}$  and  $L_{\text{H}\beta}$  vs.  $L_{\text{radio}}$  correlations, but the ionization state deduced from the emission lines does not increase with radio power as predicted by the simple, constant ISM, photionization model. We conclude that: (a) there exists a considerable range in the quasar ionizing luminosity at a given redshift; and (b) that the mean density of the emission line clouds is larger in the high redshift/high power radio sources. The latter density enhancement may either be a consequence of the increased importance of jet-cloud interactions or, alternatively, due to a higher pressure in the confining hot ISM, in the high redshift objects.

Apart from the general scatter in the correlations, we identify a distinct group of objects with [OIII] $\lambda$ 5007 luminosities which are more than order of magnitude lower than in the general population radio galaxies at similar redshift. These weak line radio galaxies (WLRG) are likely to be sources in which the central ionizing quasars are particularly feeble.

Deep spectra show that many of the sources in our sample are broad line radio galaxies (BLRG). The fact that the BLRG are observed out the redshift limit of the survey, overlapping in redshift with the quasars, argues against the idea that BLRG are simply the low radio power counterparts of high power, high redshift quasars. Either there exists a considerable range in the intrinsic luminosities of the broad-line AGN for a given redshift or radio power, or the BLRG represent partially obscured quasars. The degree of scatter present in the  $L_{\text{[OIII]}}$  vs.  $L_{\text{radio}}$  correlation supports the former possibility.

# 1 Introduction

Following the first optical identifications of extragalactic radio sources in the 1950's it became clear that powerful radio emission is associated with presence of strong optical emission lines (Baade & Minkowski 1954, Schmidt 1965). This radio-optical link is now quantified by several studies which show formal correlations between the optical emission line luminosity and the radio power (Baum & Heckman 1989, Rawlings & Saunders 1989, 1991, Morganti *et al.* 1992, Zirbel *et al.* 1995). Given that the emission line regions may be energised by EUV photons emitted in the central energy-generating region, and the radio jets have their origin in the same region, studies of the radio/optical correlations have the potential to provide fundamental information about the physics of the energy generating mechanisms in radio-loud active galaxies (see Rawlings & Saunders 1991).

The most recent studies have revealed considerable detail in the correlations. First, there is evidence that slope of the correlation between radio power and emission line luminosity is shallower for low-power FRI sources than for the more powerful FRII sources (Morganti *et al.* 1991, Zirbel *et al.* 1995), with the FRI radio sources also showing generally weaker emission lines. Second, Laing *et al.* (1994) have identified a group of galaxies which, despite being associated with powerful FRII radio sources, have only weak, low ionization emission lines (these were dubbed “low-excitation” sources). Third, Rawlings & Saunders (1991) found that they could reduce some of the scatter in the correlations by plotting radio jet power (rather than radio luminosity) against total emission line luminosity.

It has also become clear that the emission line properties may be affected by anisotropy and obscuration. Notably, radio sources with broad-line optical spectra (BLRG, quasars) have larger [OIII] luminosities than narrow-line radio galaxies of similar extended radio power (e.g. Jackson & Browne 1990). Although it was originally thought that this difference may provide evidence against the anisotropy-based unified schemes for powerful radio sources (e.g. Barthel 1989), the observation that the [OII] luminosities of the broad- and narrow-line groups are similar (Hes *et al.* 1993), has led to the suggestion that the [OIII] emission is anisotropic, with part of the [OIII] emitted in the obscured central regions. Furthermore, Laing *et al.* (1994) have found that the difference between the broad- and narrow-line objects becomes less significant when the “low-excitation” sources are excluded from the analysis.

The correlations between optical and radio properties are generally explained in terms of an illumination model in which the emission line gas is photoionized by EUV photons emitted by a central AGN, with the strength of the photoionizing continuum linked to the power in the radio jet through the physics of the central engine (e.g. Rawlings & Saunders 1991). The detail in the correlations can then be due to fundamental differences in the nature of the central engine between the different classes of extragalactic radio sources (e.g. Baum, Zirbel & O’Dea 1995).

The illumination model has several attractions. Most notably, the AGN photoionization models are successful at explaining the relative strengths of most of the stronger emission lines in the spectra (Robinson *et al.* 1987). The apparent correlation between emission line luminosity and ionization state observed in low- $z$  radio galaxies (Saunders *et al.* 1989) is also evidence that the larger emission line luminosities measured in the more powerful radio sources result from stronger ionizing continua, rather than, for example,

an increase in the covering factor of the emitting gas with radio power or redshift. Another advantage is that, if the illuminating radiation field is anisotropic — as predicted by the unified schemes — then it is possible to explain some of the other features of the sources, such as the tendency for the extended emission line regions to align along the radio axes (e.g. Baum & Heckman 1989) and the large UV polarization measured in some cases (Tadhunter *et al.* 1992). Finally, Heckman *et al.* (1994) have found a correlation between the radio and far-IR luminosities of 3CR galaxies, which provides independent evidence that the quasar luminosity is linked to the radio jet power.

However, the illumination model cannot explain all of the emission line properties of powerful radio galaxies. The highly collimated optical/UV structures which are closely aligned with the radio axes of many high redshift radio galaxies (e.g. McCarthy *et al.* 1996; Best, Rottgering & Longair 1996) are inconsistent with the illumination of a uniform halo of clouds by the broad radiation cones predicted by the unified schemes. Moreover, the extreme emission line kinematics observed in such sources are difficult to explain in terms of AGN illumination of the *undisturbed* ISM of the host galaxies (e.g. Tadhunter 1991; McCarthy *et al.* 1996). While these results do not rule out AGN illumination, they demonstrate that other mechanisms must also contribute.

Recent theoretical work has raised the possibility of a direct link between the radio plasma and the emission-line material. Sutherland *et al.* (1993) have proposed that the extended emission line filaments in Centaurus A are ionized by shocks generated in the turbulent boundary layer between the radio jets and the ISM. By tuning the models they can obtain a good fit to the general emission line spectra, and, crucially, their models provide a better fit the  $[\text{OIII}](5007+4959)/4363$  diagnostic ratio than the single slab photoionization models. This work underlines the fact that it can be difficult to distinguish between the emission line spectra produced by fast shocks and AGN photoionization, because much of the ionizing effect of a fast shocks is due to photoionization by hot post-shock gas. Although the application of Sutherland *et al.* model to the specific case of Centaurus A is controversial, since the filaments lie well outside the active inner radio jets, detailed spectroscopic studies of other jet-cloud interaction candidates demonstrate that the shock models may be more generally applicable (e.g. Clark 1996, Clark *et al.* 1997). The balance between jet-induced shocks and AGN illumination is clearly a key issue for our general understanding of the optical-radio correlations in radio galaxies.

In this paper we use spectroscopic observations of a complete sample of southern 2Jy radio galaxies to investigate the nature of the optical–radio correlations for powerful radio sources. In particular, we address the question of whether the correlations can be reconciled with the AGN illumination model.

## 2 Sample selection and data

As originally defined by Tadhunter *et al.* (1993), our complete sample consists of all sources from the 2Jy sample of Wall & Peacock (1985) with declinations  $\delta < +10^\circ$  and redshifts  $z < 0.7$ . Optical, radio and X-ray observations for the complete sample are presented in Tadhunter *et al.* (1993), Morganti *et al.* (1993) and Siebert *et al.* (1996) respectively, while new optical identifications made in the course of the survey are discussed in di

Serego Alighieri *et al.* (1994). The main advantages of this sample are that it contains a good mix of objects, it covers a wide range in redshift, and, for all the objects with redshifts  $z > 0.1$ , we have complete information about the emission line luminosities and ionization state of the emission line gas.

Since the publication of preliminary results by Tadhunter *et al.* (1993), deeper spectra have been obtained for most of the radio galaxies with redshifts  $z > 0.15$ . As well as improving the quality and completeness of the emission line data, these new observations have resulted in the detection of weak broad lines in some of the sources previously classified as narrow line radio galaxies (NLRG). Such sources are now re-classified as broad line radio galaxies (BLRG).

The identification status of the full 2Jy sample of Wall and Peacock (1985) has also improved since the earlier paper. Many of the new identifications were discussed in di Serego Alighieri *et al.* (1994). The only important change involving the  $z < 0.7$  sample is that broad line radio galaxy 0347+05 is now included. This object was originally thought to be at higher redshifts, but spectra presented by di Serego Alighieri *et al.* (1994) and Allington-Smith *et al.* (1993) place it at a redshift of  $z = 0.339$ . Otherwise, all the recent identification work has reinforced the conclusion of Tadhunter *et al.* (1993), that the completeness of the  $z < 0.7$  sample is high; the few remaining objects in the full 2Jy sample without spectroscopic redshifts are all very faint and are extremely unlikely to fall at  $z < 0.7$ .

Because of its high selection frequency (2.7GHz), the Tadhunter *et al.* (1993) sample contains a number of objects dominated by flat spectrum core radio emission. However, in order to avoiding possible orientation biases, we require a sample selected on the basis of the extended, steep spectrum radio emission. To get around this problem we have re-selected our sample as follows: the 2.7GHz core flux was first estimated from the 5GHz core flux by assuming a flat spectra index for the core component; the estimated 2.7GHz core flux was then subtracted from the total 2.7GHz flux, to find the extended flux; finally, a new sub-sample was selected which consists of objects with extended 2.7GHz flux greater than 2Jy. We will refer to the new sample selected in this way as the steep spectrum selected (SSS) subsample. As expected, the main effect of the reselection is to remove the majority of the quasars dominated by compact flat spectrum core components. With the exception of the quasar 3C273 — which would be selected at 2Jy on the basis of its steep spectrum jet emission alone — all of the objects in the SSS subsample are dominated by emission from regions with a steep high frequency radio spectrum. The reselection process is not perfect, because the core components may be variable, and the core spectra not exactly flat. However, we believe that it is adequate for the purposes of the discussion below.

Basic data for the SSS subsample, including updated spectral classifications and the latest emission line measurements, are presented in Table 1. The radio luminosities have been calculated by using the known power-law spectral index (2.7 — 5GHz) to integrate the radio spectrum over the frequency range 0.1 — 100 GHz<sup>1</sup>.

The classification of objects in Table 1 warrants a further discussion. As well as classifying the objects on the basis of the radio emission, we also classify them according

---

<sup>1</sup> $H_0 = 50 \text{ km s}^{-1} \text{ Mpc}^{-1}$ ,  $q_0 = 0.0$  are assumed throughout this paper

to their optical properties into five types: narrow line radio galaxies (NLRG), broad line radio galaxies (BLRG), quasars (Q), BL Lac objects (BL), and weak line radio galaxies (WLRG). Objects in the latter class are dominated by the absorption features of the stellar populations in the host galaxies, with small  $[\text{OIII}]\lambda 5007$  emission line equivalent widths ( $EW([\text{OIII}]) < 10\text{\AA}$ ). The dividing line between BLRG and quasars is fuzzy: both types show broad permitted lines in their optical spectra, but the quasars were originally classified as such by Wall & Peacock (1985) on the basis of their stellar appearance on optical images, whereas the BLRG were originally classified as galaxies because they appeared more diffuse. However, in our sample the absolute magnitude distributions of quasars and BLRG overlap. If we adopt the absolute magnitude criterion of Veron-Cetty & Veron (1993) for the division between quasars and active galaxies (quasars are those objects with  $M_v < -23.0$ ), then PKS1547-79 and PKS2135-20 would be re-classified as quasars, while PKS1151-34 would be re-classified as a BLRG. In Table 1 we stick with the original morphological classification of Wall & Peacock (1985).

The data in Table 1 will form the basis of much of the subsequent discussion and analysis.

## 3 Results

### 3.1 Radio-optical correlations for the full sample

Figure 1 shows the correlations between the  $[\text{OIII}]\lambda 5007$  and radio luminosities for the full  $z < 0.7$  sample of Tadhunter *et al.* (1993), including the latest emission-line data. In order to examine the possible dependence of the correlations on the radio morphology, the various radio types are indicated by different symbols.

As previously noted by Baum & Heckman (1989), the relationship between the emission line and radio luminosities is not linear. Interesting features include the following:

- **FRI radio sources.** The FRI sources are invariably classified as WLRG; they comprise the majority of upper limits in the lower left hand part of the diagram; none have strong enough emission lines to qualify as NLRG. Because of the large proportion of  $[\text{OIII}]$  upper limits amongst the FRIs, it is not possible to determine from our data whether the FRIs follow a separate correlation with a shallower slope on this diagram (e.g. Zirbel *et al.* 1995), or whether they merely form a continuation of the sequence for more powerful radio sources.
- **FRII radio sources.** While the FRII sources may follow a linear correlation at the high luminosity end of the diagram, below a radio luminosity of approximately  $10^{44} \text{ erg s}^{-1}$ , the points scatter towards the zone occupied by the FRI sources at low  $[\text{OIII}]$  luminosities. It is clear that there exists a significant population of FRII sources with low emission line luminosities (see also Laing *et al.* 1994).
- **Compact steep spectrum radio sources.** If we define compact radio sources to be those with diameters  $D < 15\text{kpc}$ , we find that the compact sources with steep high frequency radio spectra fall on the main correlation between emission line luminosity and radio luminosity; their emission line properties do not appear

significantly different from those of more extended radio sources of similar power. The emission line properties of the compact steep spectrum radio sources in the sample are discussed in more detail by Morganti *et al.* 1997.

### 3.2 The correlations for different emission lines

The incompleteness of the emission line data for the low redshift objects makes further quantitative investigation of the correlations difficult using the full Tadhunter *et al.* 1993 sample. However, beyond a redshift of  $z > 0.1$ , estimates of the [OIII] $\lambda$ 5007 and [OII] $\lambda$ 3727 luminosities exist for all quasars and galaxies, and estimates of the  $H\beta$  (narrow) luminosities are also available for most of the galaxies (but not the quasars). Thus, by restricting the redshift range to  $0.1 < z < 0.7$ , we can examine whether correlations are the same for all the emission lines.

Figures 2a,b,c show respectively the [OIII] $\lambda$ 5007, [OII] $\lambda$ 3727 and  $H\beta$  luminosities plotted against extended radio luminosity for all the objects in the SSS sub-sample with  $z > 0.1$ . Note that the scatter in these plots is real, and not simply a consequence of observational error: Tadhunter *et al.* (1993) estimated that the errors in the emission line luminosities amounted to less than a factor of two (or  $\pm 0.3$  in the log), even allowing for possible slit losses, and this is borne out by more recent repeat measurements of many of the higher redshift objects in the sample.

It is clear that, although the degree of scatter is similar for  $L_{[OII]}$  vs.  $L_{radio}$  and  $L_{H\beta}$  vs.  $L_{radio}$  plots, there is a significantly larger scatter in the  $L_{[OIII]}$  vs.  $L_{radio}$  plot. A particularly noteworthy feature is that there exists a distinct group of four objects with [OIII] luminosities which are more than a factor of ten lower than would be expected from the main correlation. This low luminosity group comprises 0043-42, 0347+05, 1648+05(Her A) and 2211-17(3C444). All of these objects have a low ionization state, and with the exception of 1648+05, which has a radio morphology somewhere between an FRI and an FRII, all the objects have an FRII radio morphology. A further interesting feature is that, despite the low *narrow* emission luminosities, one of the objects in the low luminosity group is classified as BLRG (0347+05). Presumably these low [OIII] luminosity objects form part of the class of “low excitation” objects identified in the 3C sample by Laing *et al.* 1994, although we prefer to label them weak line radio galaxies (WLRG) on the grounds that the meaning of the term “excitation” in this context is not sufficiently clear. The nature of the WLRGs will be discussed in more detail in section 4.3.

Careful comparison of Figures 2a,b,c reveals that, even if the WLRG are excluded, *the scatter remains larger in the  $L_{[OIII]}$  vs.  $L_{radio}$  correlation than in the correlations involving the other two emission lines.*

To test the significance of the correlations, we have calculated the Spearman  $\rho$  correlation coefficient for various correlations involving the three emission lines<sup>2</sup>. The results are shown in Table 2, from which it is clear that the null hypothesis that no correlation exists between emission line and radio luminosities can be rejected at a high

---

<sup>2</sup>Note that, due to the strong correlation between radio power and redshift in this radio flux limited sample, it is not possible to determine whether it is the radio power or the redshift that is the fundamental variable. For this reason the terms radio power and redshift are often interchangeable in the text

level of significance for the  $L_{[OII]}$  vs.  $L_{radio}$  correlation. However, as expected, the level of significance is lower for the  $L_{[OIII]}$  vs.  $L_{radio}$  correlation.

We have also used a linear regression analysis to calculate the slopes of the correlations assuming a linear relationship between the two variables (on log-log plots). We find the following relationships:  $L_{[OIII]} \propto (L_{radio})^{0.308 \pm 0.015}$  and  $L_{[OII]} \propto (L_{radio})^{0.576 \pm 0.010}$ . Note that in each case we have assumed that the emission line luminosity is the dependent variable. The WLRG have been excluded from this analysis, since they form a distinct group of objects which falls off the main correlations.

### 3.3 Ionization state and luminosity

Investigations of the relationship between ionization state and luminosity provide important information about the nature of the optical–radio correlations for powerful radio galaxies.

Previous results presented by Saunders *et al.* 1989 for a complete sample of low redshift radio galaxies ( $z < 0.2$ ) showed evidence for an anti-correlation between the ionization-sensitive  $[OII](3727)/[OIII](5007)$  ratio and  $L_{[OIII]}$ , implying that the more luminous objects have a higher ionization state. Our data now allow us to investigate the ionization/luminosity relationship in greater depth and, in particular, to determine whether the trends noted by Saunders *et al.* continue to higher redshifts and higher radio powers.

Figures 3a,b,c and d show  $[OII](3727)/[OIII](5007)$  plotted against  $L_{[OII]}$ ,  $L_{[OIII]}$ ,  $L_{H\beta}$  and  $L_{rad}$  respectively for the  $z > 0.1$  SSS sub-sample. The Spearman’s  $\rho$  correlation coefficients and the associated significance levels are listed in Table 2. For comparison, the data for objects in the Saunders *et al.* (1989) sample and assorted higher redshift 3C galaxies from the literature are plotted in Figure 4.

Concentrating first on  $[OII]/[OIII]$  vs.  $L_{[OIII]}$  (Figure 3a), we find that we can confirm the Saunders *et al.* result: for the lower redshift ( $0.1 < z < 0.2$ ) objects in our sample there is a definite trend of decreasing  $[OII]/[OIII]$  with  $[OIII]$  emission line luminosity. However, considering the full redshift range of our sample ( $0.1 < z < 0.7$ ), the trend is much weaker. In fact, there are signs that the slope of the relationship flattens off at high emission line luminosities, especially if the WLRG are removed. Part of the reason for the weakness of the trends for the full redshift range becomes clear when the high ( $0.2 < z < 0.7$ ) and low ( $0.1 < z < 0.2$ ) redshift objects are considered separately: with the exception of the WLRG 0347+05, the high and low redshift objects occupy separate regions of the diagram, with the high redshift objects appearing to form a parallel sequence to the low redshift objects. *It is clear that high redshift objects do not form a high ionization continuation of the correlation found for the lower redshift objects.* Similar trends are noted in Figure 4 for the 3C objects (see also Jackson & Rawlings 1997), although in this case the sample is not complete beyond a redshift of  $z = 0.2$ .

At this point it should be stressed that some care is required when interpreting the  $[OII]/[OIII]$  vs.  $L_{[OIII]}$  anti-correlation, because of the mutual dependence of both variables on the  $[OIII]$  luminosity. For example, even for the case in which the  $L_{[OII]}$  and  $L_{[OIII]}$  luminosities are uncorrelated, and there is no genuine physical correlation between ionization state and luminosity, a spurious anti-correlation would nonetheless be observed

simply because of this effect. In the case of the data plotted in Figure 3, we note that there is in fact a strong correlation between  $L_{[OIII]}$  and  $L_{[OII]}$  (Table 2), and this effect is unlikely to be the sole cause of the anti-correlation observed for the low redshift objects in Figure 3a.

It is significant that, despite the possible anti-correlation between the  $[OII]/[OIII]$  ratio and  $[OIII]\lambda 5007$  luminosity observed at low redshifts, no significant anti-correlations are found in the plots involving the other emission lines and the radio luminosity (Table 2, Figures 3b,c,d). In none of these diagrams do the high power/high redshift sources form a continuation of the sequence defined by the low power/low redshift source. This result holds for both the broad and the narrow line objects, which are indicated by different symbols in the diagram.

On balance, the evidence for a strong anti-correlation between ionization state and luminosity is weak when we consider the full redshift range of the sample. Table 3 shows the median of the measured values of  $[OII](3727)/[OIII](5007)$  ratio for different redshift ranges. It is clear from this that the median  $[OII]/[OIII]$  does not vary significantly between  $0.1 < z < 0.2$  and  $0.5 < z < 0.7$  despite more than order of magnitude increases in both the median radio luminosity and the median emission line luminosity. Indeed, the highest redshift and most luminous radio source in the sample (0409-75) has one of the lowest ionization states as indicated by the  $[OII]/[OIII]$  ratio; recent observations of high redshift 3C radio galaxies also show that many of them have relatively low ionization states (Jackson & Rawlings 1997). The implications of these results for understanding the nature of the optical–radio correlations will be discussed in section 4.1.

### 3.4 Broad line objects

In common with the recent work of Laing *et al.* (1994), we find that many of the objects in the sample prove to be BLRG when observed at sufficiently high S/N. The fact that none of these BLRG is highly polarized at UV wavelengths (see Tadhunter *et al.* 1997) indicates that we are seeing the AGN directly in these objects rather than via scattering in the ISM of the host galaxies.

We detect BLRG out to the redshift limit of our sample. This shows that BLRG are not merely the low redshift/low radio power counterparts of high redshift/high power quasars; there is an overlap in radio power ranges covered by the populations of BLRG and quasars. This implies that, either there exists a considerable range in the intrinsic luminosities of broad line AGN at a given redshift/radio power, or the range of intrinsic luminosities is small but there is a range in the extinction, with the BLRG representing partially obscured quasars. The obscuration idea is supported by spectroscopic observations of low redshift BLRG which show large Balmer decrements as well as non-stellar continua which are red when compared with quasar continua (e.g. Osterbrock, Koski & Phillips 1976). The relatively strong Paschen lines measured in some BLRG may also be consistent with large reddening (e.g. Rudy & Tokunaga 1983, Lacy *et al.* 1982), although it remains a possibility in some cases that the large Balmer decrements are due to collisional excitation effects in the BLR clouds (e.g. Kwan & Krolik 1981), and that the BLRG continua are *intrinsically* red.

Concentrating on the 32 objects in the SSS sub-sample with  $0.1 < z < 0.7$ , we find



that 14 ( $44\pm14\%$ ) are broad line objects (*i.e.* BLRG or quasars). Dividing the sample by redshift, the occurrence rate of broad line objects is  $54\pm27\%$  in the high redshift half of the sample ( $0.4 < z < 0.7$ ), and  $38\pm16\%$  in the low redshift half of the sample ( $0.1 < z < 0.4$ ). Although the relative frequency of broad line objects appears to increase with redshift, the trend is not statistically significant, given the relatively small numbers of objects in the samples. These results are entirely consistent with those obtained by Lawrence (1991) for 3CR objects in the same redshift range.

It is also important to consider whether the populations of broad- and narrow line objects have significantly different [OIII] $\lambda$ 5007 emission-line luminosities, as has been found for other samples (*e.g.* Jackson & Browne 1990). Figure 5 shows  $L_{[\text{OIII}]}$  vs.  $L_{\text{rad}}$  for the SSS sub-sample, with broad- and narrow-line objects indicated by different symbols. While there may be some weak evidence from this diagram for the broad line objects to show higher [OIII] $\lambda$ 5007 luminosities, this result is not as strong as found in some previous studies. Using a Kolmogorov-Smirnov two sample test we find that the significance of the difference in the distributions of [OIII] $\lambda$ 5007 luminosities for broad- and narrow-line objects in the SSS sub-sample is only 10%. In line with the results of Laing *et al.* (1994), the differences become even less significant if the WLRG are removed from the analysis.

## 4 Discussion

### 4.1 Testing the AGN illumination model

It is generally assumed that the emission line properties of the powerful radio galaxies can be explained in terms of a quasar illumination model.

In what we will refer to as the basic quasar illumination model, the emission line regions are assumed to be photoionized by EUV photons from a central illuminating quasar or AGN; and the properties of the ISM (*e.g.* density, covering factor *etc.*) are assumed not to vary on average with redshift or radio power, although there may be a scatter in the ISM properties at a given redshift. In this model the correlations between emission line luminosity and radio power arise because of the photoionizing luminosity of the illuminating quasar and the radio jet power are tied through the physics of the central engine. We now examine whether this basic model be reconciled with the spectroscopic data.

As a starting point we consider the behaviour of the emission line flux and line ratios for a single, low density, optically thick slab of solar abundances, as the strength of the ionizing continuum is increased. The model results were generated using the MAPPINGS photoionization code for a power-law ionizing continuum shape ( $F_\nu \propto \nu^{+\alpha}$ ), and are quantified as sequences in the ionization parameter defined by:  $U = F_{\text{ion}}/n_e c$ , where  $F_{\text{ion}}$  is the number of ionizing photons per unit area at the face of the slab,  $n_e$  is the electron density in the cloud, and  $c$  is the speed of light. The models make the following general predictions:

- **Variation in [OIII] $\lambda$ 5007 luminosity with ionizing continuum luminosity.** Over the range of ionization parameter consistent with the emission line ratios measured in low redshift radio galaxies ( $10^{-3} < U < 10^{-1}$ : Robinson *et al.* 1987)

the [OIII] luminosity rises steeply with the ionizing continuum luminosity ( $L_{[OIII]} \propto (L_{ion})^{+\beta}$  with  $\beta = 1.2$  for  $\alpha = -1.5$ ). This result holds for a wide range of ionizing continuum shapes ( $1.1 < \beta < 1.3$  for  $-1.0 > \alpha > -2.0$ ).

- **Variation in [OII] $\lambda$ 3727 luminosity with ionizing continuum luminosity.** Over a similar range of ionization parameter, the [OII] $\lambda$ 3727 luminosity rises much less steeply with ionizing continuum luminosity than the [OIII] $\lambda$ 5007 luminosity ( $L_{[OII]} \propto (L_{ion})^{+\beta}$  with  $\beta = 0.46$  for  $\alpha = -1.5$ ). In this case there is a larger variation in the slope of the relationship with the shape of the ionizing continuum ( $0.8 < \beta < 0.4$  for  $-1.0 > \alpha > -2.0$ ), but the slope is always predicted to be less than in the case of the relationships between  $L_{[OIII]}$  and  $L_{ion}$ .
- **Variation of ionization state with ionizing continuum luminosity.** The ionization state is predicted to increase as the ionizing continuum luminosity is increased at fixed  $n_e$ . In consequence, the [OII](3727)/[OIII](5007) ionization diagnostic ratio will decrease as both the [OIII] and [OII] emission line luminosities increase, but the rate of decrease of [OII]/[OIII] is predicted to be significantly steeper with [OII] than with [OIII] ( $[OII]/[OIII] \propto (L_{[OIII]})^{-0.64}$  and  $[OII]/[OIII] \propto (L_{[OII]})^{-1.7}$  for an  $\alpha = -1.5$  ionizing continuum).
- **Diagnostic diagrams.** The models form unique sequences in the ionization parameter on the diagnostic diagrams, with the position of each sequence depending on the shape of the ionizing continuum (e.g. Robinson *et al.* 1987).

We emphasise that these results were derived from single slab models. In reality, our spectroscopic observations will encompass an ensemble of emission line clouds in each radio galaxy, covering a wide range of radii and density. However, provided that the condition of the clouds being optically thick holds, and the densities do not become so high that collisional de-excitation effects become important, then we expect these predictions to apply to ensembles of clouds: the ensemble as a whole will move up and down the ionization parameter sequences as the ionizing continuum luminosity is varied.

At least some features of our observations are consistent with the single slab photoionization models. Figure 6 shows the [OII](3727)/[OIII](5007) vs. [OIII](5007)/H $\beta$  diagnostic diagram with data points from the  $z > 0.1$  SSS subsample compared with the photoionization model predictions for various photoionizing continuum shapes. With the exception of some of the extreme low ionization points, the data points form a tight sequence on this diagram, with a power-law photoionization model providing the best fit to the data for a spectral index  $\alpha = -1.5$ . This is entirely consistent with the results obtained for a sample of low redshift radio galaxies by Robinson *et al.* (1987), despite the fact that the current sample extends to much higher redshifts and radio powers. Note, however, that this agreement with the photoionization model predictions does not rule out other ionization mechanisms: the predictions of fast shock models overlap with the predictions of the photoionization models in some sectors of the diagnostic diagrams (e.g. Sutherland *et al.* 1993).

The photoionization models also provide a ready explanation for the increased scatter in the  $L_{[OIII]}$  vs.  $L_{radio}$  correlation relative to the correlations involving the other

emission lines. If the scatter in the emission line luminosity reflects a range in intrinsic quasar ionizing luminosities at a given radio power, then the photoionization models predict a greater scatter in the  $L_{[OIII]}$  vs.  $L_{radio}$  diagram, because the  $[OIII]$  emission lines are more sensitive to variations in the ionizing continuum than the  $[OII]$  lines over the relevant range of ionization parameter. This effect also explains why the WLRGs fall well below the locus of points for the other radio galaxies in the  $L_{[OIII]}$  vs.  $L_{radio}$  diagram, but fall much closer to the locus in the  $L_{[OII]}$  vs.  $L_{radio}$  diagram. Note that the data allow us to rule out the possibility that the scatter in the correlations is solely due to a variation in the covering factor of the emission line clouds, since a variation of the covering factor would affect  $[OIII]\lambda 5007$ ,  $[OII]\lambda 3727$  and  $H\beta$  equally, and the scatter would be the same in all the correlations.

The evidence to support the quasar illumination model based on the slopes of the correlations between radio power and emission line luminosity is more ambiguous. Although all the emission line luminosities increase with radio luminosity, as expected in the case of a direct link between the luminosity in the quasar ionizing continuum and the radio jet power, the  $[OII]$  luminosity appears to increase more rapidly with the radio luminosity than the  $[OIII]$  luminosity (section 3.2, Figure 2), in apparent contradiction of the photoionization model results. However, given the large scatter and relatively low significance of the  $L_{[OIII]}$  vs.  $L_{radio}$  correlation, this does not by itself represent strong evidence against the quasar illumination model. Furthermore, the slope of the  $L_{[OII]}$  vs.  $L_{radio}$  correlation is not far from the prediction of the quasar illumination model.

More worrying for the basic illumination model is the lack of evidence for a strong anti-correlation between the ionization-sensitive  $[OII](3727)/[OIII](5007)$  ratio and the emission line luminosity (see section 3.3). On the basis of the single slab model, we would expect the high power objects at high redshifts to form a high ionization extension to any correlation found for the low redshift sources, but in fact the high redshift sources form a parallel locus in the diagrams, and cover a similar range in ionization to the low redshift sources (Table 3).

Thus, although the basic quasar illumination model is successful in some aspects, it cannot explain all the features of our data. We now consider the alternatives.

## 4.2 Modifications to the quasar illumination model

We emphasise that failure of the quasar illumination model to explain all features of the data does not imply that the general idea of photoionization of the emission line clouds by the quasar nucleus should be abandoned. If the unified schemes for radio-loud active galaxies are correct, then all powerful radio galaxies will harbour luminous quasars in their cores which, for typical ISM properties, will have a significant effect on the ionization of the emission line clouds. Quasar illumination is also supported by the detection of scattered UV continuum emission and broad lines in the extended nebulosities of many powerful radio galaxies (e.g. Cimatti *et al.* 1995, Young *et al.* 1996), including some objects from the SSS (Tadhunter *et al.* 1997); such polarized features cannot not be produced in any other way than quasar illumination.

Rather we should look to the assumptions of the simple illumination model, and consider what modifications are required to bring the illumination model into agreement

with the observations.

First, we consider the assumptions of the single slab photoionization models. In the above discussion it was assumed that the photoionized clouds are large enough to be optically thick to the photoionizing continuum (*i.e.* radiation bounded). Relaxation of this assumption could lead to a decrease in the strength of  $[\text{OII}]\lambda 3727$  relative to  $[\text{OIII}]\lambda 5007$ , because optically thin clouds have less extensive partially ionized zones in which low ionization lines such as  $[\text{OII}]\lambda 3727$  are produced. Thus, in order to explain the relatively strong  $[\text{OII}]$  emission in the high redshift objects we require that the clouds become more optically thick as the radio power and redshift are increased. However, if the ISM properties are the same on average at all radio powers and redshifts, then it is inevitable that, as the quasar ionizing continuum luminosity is increased we will observe *more* optically thin clouds in the higher power sources — the reverse of what we would require to explain the stronger  $[\text{OII}]$  emission by this mechanism.

A major assumption of the simple quasar illumination model is that, on average, the properties of the ISM do not change as a function of redshift or radio power. A plausible explanation for the relatively strong  $[\text{OII}]$ , and high  $[\text{OII}]/[\text{OIII}]$  ratios observed in the high redshift objects is that, in reality, there is significant evolution in the density distribution of the clouds as a function of redshift or radio power. For a given ionizing luminosity and radius from the ionizing source, the ionization state of the gas is inversely proportional to the density. Thus, an increase in the mean density of the emitting clouds with radio power or redshift could compensate for the increase in the strength of the ionizing continuum, and ensure that the range of ionization observed in high and low redshift objects is similar. Such a change in the density is plausible and might arise in two ways:

- **Evolution in the environment and confining medium.** It is generally assumed that the warm emission line clouds are confined by a hot X-ray emitting phase of the ISM associated with the host galaxy (*e.g.* Forman, Jones & Tucker 1985) or cluster of galaxies (*e.g.* Fabian, Nulsen & Canizares 1984). In this case, the density of the warm clouds will be related to the pressure of the hot confining medium, which will be larger close to the centres of rich clusters of galaxies than close to the centres of isolated galaxies. Thus, it is plausible that the high redshift/high power sources have larger gas densities because they are in richer environments than their low redshift/low power counterparts. Indeed, optical imaging studies of the fields of radio galaxies provide strong evidence for the required evolution in the radio source environments (Hill & Lilly 1991), while X-ray observations of at least some powerful high redshift radio galaxies show direct evidence for a high pressure IGM (Crawford & Fabian 1994, 1996). The fact that the nearby powerful radio galaxy Cygnus A — one of the few nearby radio galaxies of comparable power to the high redshift radio galaxies — also lies at the heart of a rich cluster with a dense IGM, suggests that the evolution in the environments is an evolution with radio power rather than redshift. It is also notable that the relatively large  $[\text{OII}]/[\text{OIII}]$  ratios measured in extended emission line regions around radio-loud quasars have been used to *deduce* the presence of a high pressure confining medium at high redshifts (Crawford & Fabian 1989, Forbes *et al.* 1990).

- **The compression effect of jet-cloud interactions.** Gas along the radio axes will be compressed as it passes through the shocks driven through the ISM by the radio jets and enters the jet cocoon (the gas may also be ionized as it passes through the shocks — see below), with typical compression factors of order  $\times 100$  or more. Hence, if the jet-cloud interactions become more important in the high redshift sources, the densities will be higher, the ionization state lower, and the  $[\text{OII}]\lambda 3727$  relatively stronger. This is before considering the additional ionizing effects of the jet shocks (see below). There is now plenty of evidence to support the idea that the jet-cloud interactions become relatively more important as the redshift increases: not only do the extended structures become more closely aligned with the radio axes (e.g. McCarthy *et al.* 1987), but the emission line kinematics become more extreme as the redshift increases (McCarthy *et al.* 1996). Furthermore, accurate measurements of densities and pressures in the EELR along the radio axes of nearby radio galaxies provide direct evidence for pressures significantly greater than indicated by X-ray observations of the hot ISM in the same galaxies (Clark 1996, Clark & Tadhunter 1996). Recently Best *et al.* (1997) have found evidence for a correlation between the optical/UV morphologies of the high redshift radio galaxies and the diameters of the radio sources, in the sense that the objects with the highest surface brightness, most closely aligned structures have the most compact radio sources. In the context of the jet-cloud interaction model these results can be explained in terms of an increasing dominance of the jet-induced shocks in the more compact sources. Indeed it is notable that two of the high redshift sources in Best *et al.* with compact radio sources and closely aligned radio and optical structures — 3C368 and 3C324 — have relatively low ionization emission line spectra ( $[\text{OII}](3727)/[\text{OIII}](5007) \sim 1$  Jackson & Rawlings 1997), consistent with the dominance of jet-induced shocks, whereas the one object with a broad, roughly bi-conical emission line distribution and relatively extended radio source — 3C265 — has a high ionization emission line spectrum, consistent with the dominance of AGN illumination of the ambient ISM (see Figure 4). It will be important in the future to investigate in more detail the links between the alignment effect, the compactness of the radio source and the ionization state of the emission line gas.

An alternative possibility is that, due to the particular combination of the radial density law and geometrical dilution of the radiation field, the ionization state of the gas decreases with radius. Then, if the mean radial distance of the emitting clouds from the nucleus is larger at high redshifts, lower ionization states will result than in the constant radius situation. Such a situation might arise, for example, if the warm gas originates in mergers, but has yet to settle into a stable configuration in the central regions of the host galaxies of the high redshift sources. Alternatively, the emission line clouds at small radii could be more heavily obscured by the central dust lane in the higher redshift sources. The published data on the emission line structures of powerful radio galaxies do show some evidence for a change in the distribution of emission lines with redshift: whereas the emission lines in most low redshift radio galaxies show a strong, dominant peak in the emission line distribution centred on the continuum nucleus (Tadhunter 1987, Baum *et al.* 1988), the emission lines in high redshift radio galaxies ( $z > 0.5$ ) often peak well away from the continuum nucleus, with a large fraction of the emission line flux emitted

outside a radius of 10kpc (McCarthy *et al.* 1996). However, it is not yet clear whether this change in the emission line distribution is another manifestation of jet-cloud interactions, which become more important at high redshifts, or reflects a real change in the intrinsic distribution of warm/cool interstellar medium with redshift or radio power.

It is clear that the observed correlations between optical emission line and radio properties can be reconciled with the illumination model provided that the mean density and/or radial distribution of the emitting clouds evolve with redshift or radio power.

### 4.3 Alternative models

Given the close alignments between optical and radio structures and the extreme emission line kinematics observed in some sources, an obvious alternative to AGN illumination is ionization by the shocks driven through the ISM by the radio jets.

One effect of the jet shocks will be to compress the warm clouds. This will inevitably lead to a lower ionization state, even if an illuminating quasar provides the bulk of the ionizing energy. What is less clear is whether the shocks can also provide the bulk of the ionizing energy for the clouds. If they do, then the relationship between the radio and optical components is more direct than implied by the simple illumination model.

In this context it is instructive to consider the cases of low redshift radio galaxies in which there is clear evidence for detailed associations between extended emission line regions (EELR) and radio structures (see Clark 1996). In such cases emission line diagnostics not only provide direct evidence for the compression effect of the jet shocks, but, in addition, certain of the diagnostic ratios – notably  $\text{HeII}(4868)/\text{H}\beta$  and  $[\text{OIII}]\lambda 4363/(5007+4959)$  — are more consistent with shocks than with photoionization. It is important to note however that the emission line gas is roughly co-spatial with the radio structures in these objects, whereas for this paper we are considering the near-nuclear emission line regions ( $r < 20$  kpc) which are often on a much smaller scale than the extended radio structures (with the notable exception of the CSS sources).

Although there is little direct, morphological evidence for jet-cloud interactions in the near-nuclear regions, this does not rule out a significant ionizing input from the jet shocks, which could be driven tangentially through the ISM. Detailed observations of the kpc-scale gas in the powerful nearby radio galaxy Cygnus A, reveal extreme high velocity components which would be difficult to explain in any other way than jet-cloud interactions (Tadhunter 1991). Furthermore, the spatial variations in some of the emission line ratios in the same source (notably  $[\text{NII}]\lambda 6584/\text{H}\alpha$ ) defy explanation in terms of a simple AGN illumination picture (Tadhunter *et al.* 1994).

Set against the evidence for jet-cloud interactions is the strong evidence for AGN illumination. This includes: the polarimetric evidence for scattered quasars in several powerful radio galaxies; the fact that extended emission line gas in most low redshift galaxies lies well away from the radio axis and has relatively quiescent kinematics; and the emission line diagnostic diagrams. Note that, although the success of the photoionization models in the diagnostic diagrams does not rule out other ionization mechanisms — the results of the shock and photoionization models overlap in some regions of the diagnostic diagrams — pure photoionization models can explain the *sequences* on these diagrams more naturally than pure shock models.

If we were to abandon AGN photoionization entirely, it would then be difficult to explain the good correlations between radio and optical emission line luminosities by shocks alone. Variable factors in the shock models include the distribution of gas relative to the radio structures, the shock speed, and the relative importance of precursor gas and shocked gas. While it is true that the radio jets are likely to be more powerful in the more luminous radio sources, it is not at all clear that this will translate into a good correlation between emission line luminosity and radio power via jet-cloud interactions.

Given that the closer UV/radio alignments and the more extreme emission line kinematics observed in the high redshift radio galaxies, it is plausible that the jet shocks become an increasingly important source of ionizing energy as the radio power or redshift increase. Since the shocks can produce a relatively low ionization state, the shock ionization might also help to explain the lower-than-expected ionization states observed in the higher redshift objects.

However, it is unlikely that the jets provide the bulk of the ionizing energy over the entire range of radio power and redshift.

#### 4.4 The nature of the WLRG

In section 3.2 we identified a distinct group of weak line radio galaxies (WLRG) with  $[\text{OIII}]\lambda 5007$  luminosities more than a factor of ten below those of the general population of radio galaxies at similar redshifts. All of these WLRG also show a low ionization state, as indicated by the  $[\text{OII}](3727)/[\text{OIII}](5007)$  ratio. How do we explain the low  $[\text{OIII}]\lambda 5007$  luminosities of these objects? In the context of the quasar illumination model there are several possibilities:

- (a) The illuminating quasars are much weaker in the WLRG.
- (b) The covering factor of the emission line clouds is lower.
- (c) The gas density is much higher than average, and this leads to lower ionization state, and relatively weaker  $[\text{OIII}]\lambda 5007$  emission.
- (d) The radio sources are over-luminous (e.g. Barthel & Arnaud 1997).

The lower covering factors idea (possibility (b)) cannot work by itself because, while lower covering factors will lead to lower emission line luminosities, this would not explain the lower ionization states observed in the WLRG. It is also clear that higher densities (possibility (c)) cannot be the sole cause of the lower  $[\text{OIII}]\lambda 5007$  luminosities, because the  $\text{H}\beta$  luminosities — which are a direct measure of the number of ionizing photons intercepted by the clouds — are also significantly lower than the mean in at least two of the sources (2211-17 and 1648+05).

An alternative explanation is that emission line clouds in WLRG have both a higher density *and* a lower covering factor than the general population of powerful radio galaxies (*i.e.* a combination of (b) and (d)). If the emission line clouds are spherical and have the same mass distribution on average in all radio galaxies, then such a combination could arise because the pressure in the hot confining medium is much larger in the WLRG: the density will rise and the covering factor will decrease as the confining pressure increases.

The lower ionization states measured in the WLRG imply a density and pressure that are a factor of  $\sim 10$  higher than in the general population of powerful radio galaxies, for a given AGN luminosity. Since the covering factors of the spherical clouds scale as  $(\text{pressure})^{-2/3}$ , a factor  $\sim 10$  increase in density and pressure implies a factor  $\sim 5$  decrease in the covering factor. Such a decrease is consistent with the lower  $H\beta$  luminosities of WLRG.

Another explanation related to the environments of the sources is that, rather than the emission lines being under-luminous, the radio sources are over-luminous, due to their interaction with the dense, hot interstellar medium in rich clusters of galaxies (possibility (d): see Barthel & Arnaud 1996). In this context it is notable that 1648+05 and 2211-17 are the among the most luminous X-ray sources in the SSS subsample, with direct evidence for extended, high-pressure X-ray haloes (Siebert *et al.* 1996). On the other hand, while the X-ray observations of 0347+05 are inconclusive, the X-ray observations of 0043-42 show no evidence for a dense confining medium. In addition, at least some powerful radio galaxies in dense environments show strong, high ionization emission lines (e.g. Cygnus A: Tadhunter *et al.* 1994).

Although the relationship between the emission line luminosity and the environment requires further investigation, the simplest explanation for the properties of the WLRG is that the illuminating AGN in these sources are an order of magnitude less powerful than in the general population of radio galaxies at similar redshifts (possibility (a)). If correct, this explanation would have important implications for the unified schemes because it would imply that not all powerful radio galaxies have luminous quasars in their cores.

## 4.5 Implications for the unified schemes

In a statistical sense our observations support the anisotropy-based unified schemes for powerful radio sources: the proportion of broad line objects in the SSS is comparable to that found in samples of 3C radio galaxies; the implied opening angle for the quasar radiation cone ( $56 \pm 10^\circ$ ) is consistent with estimates based on comparison of the linear size distributions of 3C quasars and radio galaxies (Barthel 1989); and the differences between the [OIII] luminosities of broad and narrow line objects in our sample are small, especially when the WLRG are removed from the analysis. In a recent analysis of the core radio emission of sources in the SSS subsample, Morganti *et al.* 1996 found that the broad line objects show a tendency to have relatively stronger radio cores than the narrow line objects in the same sample, where the relative core strength ( $R$ ) is quantified as the ratio of core to extended radio flux at a particular frequency. (i.e.  $R = S_{\text{core}}/S_{\text{ext}}$ ). Again this is consistent with the anisotropy-based unified schemes in which the radio core emission is strongly anisotropic due to relativistic beaming effects.

Despite the positive *statistical* evidence, there are individual objects which cannot be readily accommodated within the unified schemes. Two objects stand out: PKS0347+05 and PKS1549-79<sup>3</sup>. On the basis of unified schemes we expect the objects with the radio axes pointing close to the line of sight to have optical spectra dominated by broad lines and relatively strong radio cores (i.e. large  $R$ ), while the objects with radio axes close to the sky plane should have optical spectra dominated by narrow lines and relatively weak radio

---

<sup>3</sup>Note that PKS1549-79 is part of the Tadhunter *et al.* (1993) sample, but it is excluded from the SSS sub-sample because its radio emission is dominated by a flat spectrum core component



cores (small  $R$ ). However, PKS0347+05 has extremely weak radio core ( $R_{2.3GHz} < 0.0006$ ) yet its optical spectrum is dominated by broad lines with only weak narrow lines, whereas in the case of PKS1549-79 we find an extremely strong radio core ( $R_{2.3GHz} = 1.310$ ), strong narrow lines, but no sign of broad permitted lines. In showing exactly the reverse pattern of behaviour to that predicted by the unified schemes, these objects provide a timely reminder that the unified schemes, if they have any validity, are only valid in a statistic sense; the quasar cone opening angles, intrinsic quasar luminosities, bulk jet powers and ISM properties are likely to vary considerably from source to source. The existence of a group of objects in which the illuminating quasar emission is apparently weak or non-existent (the WLRG), further emphasises this point.

## 5 Conclusions

In line with previous results, we find strong, formal correlations between the optical emission line luminosity and the radio luminosity for our complete sample of southern 2Jy radio sources. A major new result is that different emission lines show different behaviours: the scatter in the  $L_{[OIII]}$  vs.  $L_{radio}$  correlation is greater than in either the  $L_{[OII]}$  vs.  $L_{radio}$  or the  $L_{H\beta}$  vs.  $L_{radio}$  correlations. There also exists a distinct group of objects (the WLRG) in which the  $[OIII]$  luminosity is more than an order of magnitude less than in the general population of powerful radio galaxies with similar radio power. In the context of the quasar illumination model the most natural explanation for these results is that there exists a considerable range of quasar luminosity for a given radio power, and not all powerful radio galaxies contain luminous quasars.

In the simplest quasar illumination model the correlations between radio and optical luminosities are explained in terms of the power of the photoionizing quasar increasing in proportion to the radio jet power, with the properties of the ISM remaining constant (on average) as the radio power is increased. We have made a critical test of this simple model by comparing our results with single slab photoionization models. We find that the high redshift/high radio power objects do not form a high ionization extension to the correlation between ionization and luminosity found for the low redshift radio galaxies; the range of ionization measured in the high redshift ( $0.5 < z < 0.7$ ) objects is not significantly different from that measured in the lower power, low redshift ( $0.1 < z < 0.2$ ) objects. These results can be reconciled with the simple quasar illumination model provided that the radial distribution and/or the mean density of emission line clouds varies with radio power or redshift. Density enhancements could arise because either the higher power objects are in richer cluster environments with a higher pressure confining ISM, or the compression effect of shocks driven through the ISM by the radio jets becomes increasingly important as the redshift and radio power increase. Given the strong evidence for jet/cloud interactions in many of the high redshift radio galaxies, we favour the latter explanation.

**Acknowledgments.** This work is based on observations taken using the European Southern Observatory 3.6m telescope, La Silla, Chile. We thank the STARLINK project for the support of computer facilities in Sheffield. MVM and RD acknowledge support from PPARC. RAEF is affiliated to the Astrophysics Division, Space Science Department, Eu-

ropean Space Agency.

## References

- Allington-Smith, J.R., Peacock, J.A., Dunlop, J.S., MNRAS, 1991, 253, 287
- Baade, W., Minkowski, R., 1954, ApJ, 119, 215
- Barthel, P.D., 1989, ApJ, 336, 606
- Barthel, P.D., Arnaud, K.A., 1996, MNRAS, 283, L45
- Baum, S.A., Heckman, T., Bridle, A.H., van Breugel, W., Miley, G., 1988, ApJS, 68, 643
- Baum, S., Heckman, T., 1989, ApJ, 336, 702
- Baum, S.A., Zirbel, E.L., O'Dea, C.P., 1995, ApJ, 451, 88
- Best, P., Longair, M., Rottgering, H., 1996, MNRAS, 280, L9
- Cimatti, A., Dey, A., van Breugel, W., Antonucci, R., Spinrad, H., 1995, ApJ, 465, 145.
- Clark, N.E., Tadhunter, C.N., 1996. In: *Cygnus A – Study of a Radio Galaxy* (eds Carilli, C.L. & Harris D.E.), CUP, p15
- Clark, N.E., 1996, PhD Thesis, University of Sheffield
- Clark, N.E., Tadhunter, C.N., Morganti, R.M., Killeen, N.E.B., Fosbury, R.A.E., Hook, R.N., Siebert, J., Shaw, M.A., 1997, MNRAS, 286, 558
- Crawford, C.S., Fabian, A.C., 1989, MNRAS, 239, 219
- Crawford, C.S., Fabian, A.C., 1993, MNRAS, 260, L15
- Crawford, C.S., Fabian, A.C., 1995, MNRAS, 273, 827
- Dickson, R.D., 1997, PhD thesis, University of Sheffield
- di Serego Alighieri, S., Danziger, I.J., Morganti, R., Tadhunter, C.N., 1994, MNRAS, 269, 998
- Fabian, C.N., Nulsen, P.E.J., Canizares, C.R., 1984, Nature, 216, 733
- Forbes, D.A., Crawford, C.S., Fabian, A.C., Johnstone, R.M., 1990, MNRAS, 244, 680
- Forman, W., Jones, C., Tucker, W., 1985, ApJ, 293, 102
- Heckman, T.M., O'Dea, C.P., Baum, S.A., Laurikainen, E., 1994, ApJ, 428, 67
- Hes, R., Barthel, P., Fosbury, 1993, Nature, 362, 326
- Hill, G., Lilly, S.J., 1991, ApJ, 367, 1

- Jackson, N., Browne, I.W.A., 1990, *Nature*, 343, 43
- Jackson, N., Rawlings, S., 1997. *MNRAS*, 286, 241
- Kwan, J., Krolik, J.H., 1981, *ApJ*, 250, 478
- Laing, R.A., Jenkins, C.R., Wall, J.V., Unger, S.W., 1994, In: *1st Stromlo Symposium on the Physics of Active Galaxies*, Bicknell, G.V., Dopita, M.A., Quinn, P.J. eds, ASP Conference Series, 54, p227
- Lacy, J.H., Soifer, B.T., Neugebauer, G., Matthews, K., Malkan, M.A., Becklin, E.E., Wu, C.-C., Boggess, A., Gull, T.R., 1982, *ApJ*, 256, 75
- Lawrence, A., 1991, *MNRAS*, 252, 586
- McCarthy, P.J., van Breugel, W.J.M., Spinrad, H., Djorgovski, S., 1987, *ApJ*, 321, L29
- McCarthy, P.J., 1993, *ARA&A*, 31, 639
- McCarthy, P., Baum, S., Spinrad, H., 1996, *ApJS*, 99, 27.
- Morganti, R., Ulrich, M.-H., Tadhunter, 1992, *MNRAS*, 254, 546
- Morganti, R., Killeen, N., Tadhunter, C.N., 1993, *MNRAS*, 263, 1023
- Morganti, R., Oosterloo, T., Reynolds, J.E., Tadhunter, C.N., Migenes, V., 1997, *MNRAS*, 284, 541
- Morganti, R., Tadhunter, C.N., Dickson, R., 1997, *A&A*, 326, 130
- Osterbrock, D.E., Koski, A.T., Phillips, M.M., 1976, *ApJ*, 206, 898
- Rawlings, S., Saunders, R., Eales, S.A., Mackay, C.D., 1989, *MNRAS*, 240, 701
- Rawlings, S., Saunders, R., 1991, *Nature*, 349, 138
- Robinson, A., Binette, L., Fosbury, R.E.A., Tadhunter, C.N., 1987, *MNRAS*, 227, 97
- Rudy, R.J., Tokunaga, A.T., 1982, *ApJ*, 256 L1
- Saunders, R., Baldwin, J.E., Rawlings, S., Warner, P.J., Miller, L., 1989, *MNRAS*, 238, 777
- Schmidt, M., 1965, *ApJ*, 141, 1
- Siebert, J., Brinkmann, W., Morganti, R., Tadhunter, C.N., Danziger, I.J., Fosbury, R.A.E., di Serego Alighieri, S., 1996, *MNRAS*, 279, 1331
- Sutherland, R., Bicknell, G.V., Dopita, M.A., 1993, *ApJ*, 414, 510
- Tadhunter, C.N., 1987, DPhil Thesis, University of Sussex.

- Tadhunter, C.N., Robinson, A., Morganti, R., 1989. In: *ESO Workshop on Extranuclear Activity in Galaxies*, eds Meurs, E.J.A., Fosbury, R.A.E., ESO Conf. and Workshop Proc. No.32, Garching, p293.
- Tadhunter, C.N., 1991, MNRAS, 251, 46p
- Tadhunter, C.N., Scarrott, S.M., Draper, P., Rolph, C., 1992, MNRAS, 256, 53p
- Tadhunter, C.N., Morganti, R.M., di Serego Alighieri, S., Fosbury, R.A.E., Danziger, I.J., 1993, MNRAS, 263, 999
- Tadhunter, C.N., Metz, S., Robinson, A., 1994, MNRAS, 268, 989
- Tadhunter, C.N., Dickson, R., Villar-Martin, M., Morganti, 1997. In: *ESO/IAC Workshop on Quasar Hosts*, Clements et al. (eds), p.311
- Véron-Cetty, M.-P., Véron, P., 1993. *A catalogue of quasars and active galactic nuclei (6th edition)*, ESO Scientific Report No.13, ESO Publications.
- Villar-Martin, M., Tadhunter, C., Morganti, R., Killeen, N., Clark, N., Axon, D., A&A, 332, 479
- Wall, J., Peacock, J., 1985, MNRAS, 216, 173
- Young, S., Hough, J.H., Efstathiou, A., Wills, B.J., Bailey, J.A., Ward, M.J., 1996, MNRAS, 279, L72
- Zirbel, E.L., Baum, S.A., 1995, ApJ, 448, 521

## Figure Captions

**Figure 1.** The correlation between [OIII] $\lambda$ 5007 emission line luminosity and total radio luminosity for the full  $z < 0.7$  sample of Tadhunter *et al.* (1993) presented as a log-log plot (the units of the luminosities are  $\text{erg s}^{-1}$ ). The objects are classified according to their radio properties as follows: filled circles — Fanaroff Riley type II; open circles — Fanaroff Riley type I; stars — compact steep spectrum radio sources with  $D < 15\text{kpc}$ ; filled triangles — compact flat spectrum radio sources; open diamonds — uncertain radio classifications. The arrows indicate objects for which we have only an upper limit in the [OIII] $\lambda$ 5007 luminosity.

**Figure 2.** The correlations between the total radio luminosity and (a) the [OIII] $\lambda$ 5007, (b) [OII] $\lambda$ 3727, and (c)  $H\beta$  emission line luminosities for the  $0.1 < z < 0.7$  SSS subsample (see text for definition). The correlations are presented as log-log plots (luminosity units:  $\text{erg s}^{-1}$ ). The symbols have the same definition as in Figure 1.

**Figure 3.** The ionization-sensitive [OII](3727)/[OIII](5007) emission line ratio plotted against: (a) [OIII] $\lambda$ 5007 luminosity, (b) [OII] $\lambda$ 3727 luminosity, (c)  $H\beta$  luminosity, and (d) total radio luminosity for the  $0.1 < z < 0.7$  SSS sub-sample (log-log plots). High redshift ( $0.2 < z < 0.7$ ) and low redshift ( $0.1 < z < 0.2$ ) objects are indicated by filled and open symbols respectively; broad line objects are indicated by circles and narrow line objects by squares. Note the separation of high and low redshift objects.

**Figure 4.** The ionization-sensitive [OII](3727)/[OIII](5007) emission line ratio plotted against [OIII] $\lambda$ 5007 emission line luminosity for 3C radio galaxies (the symbols have the same meaning as Figure 3). The data for the low redshift ( $z < 0.2$ ) objects were taken from Saunders *et al.* (1989), while the data for the higher redshift objects were taken from Dickson (1997) and Jackson & Rawlings (1997). 3C324, 3C368 and 3C265 are identified in the diagram to emphasise a possible link between ionization state and radio/optical structure. 3C324 and 3C368 have relatively compact radio sources and closely aligned radio and UV structures, whereas 3C265 has a more extended radio source and a broader, roughly biconical, emission line distribution.

**Figure 5.** The correlation between [OIII] $\lambda$ 5007 emission line luminosity and total radio luminosity for the  $0.1 < z < 0.7$  SSS sub-sample (log-log plot) with the broad line objects (including BLRG and quasars) and narrow line objects indicated by open and filled circles respectively.

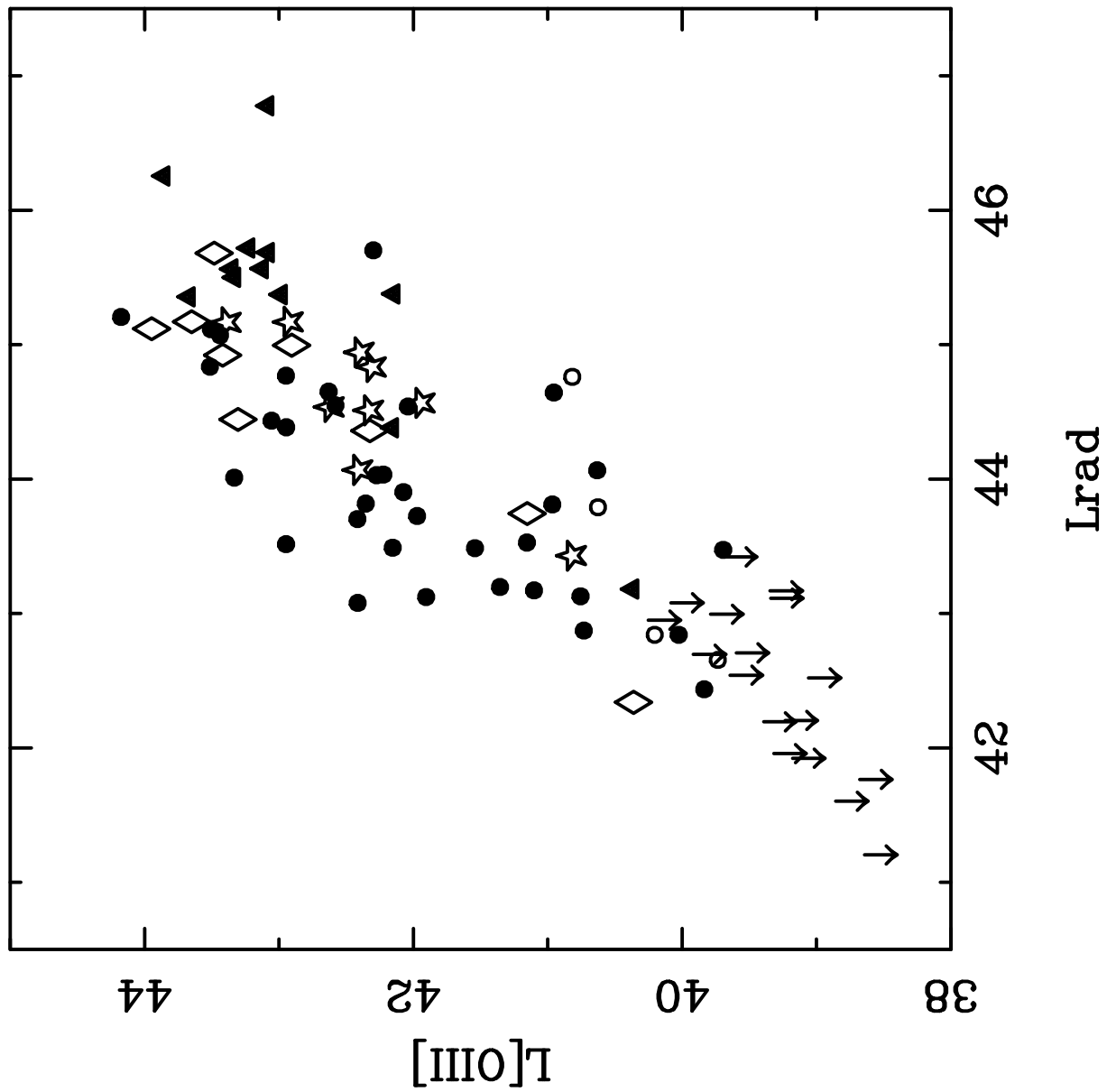
**Figure 6.** [OIII](5007)/ $H\beta$  vs. [OII](3727)/[OIII](5007) diagnostic diagram for the  $0.1 < z < 0.7$  SSS sub-sample. The results of power-law  $F_\nu \propto \nu^{+\alpha}$  photoionization model calculations are shown as sequences in the ionization parameter ( $10^{-1} < U < 10^{-4}$ , decreasing left to right) for three different ionizing continuum shapes:  $\alpha = -1.0$  (dotted line),  $\alpha = -1.5$  (dashed line), and  $\alpha = -2.0$  (dot-dashed line). Broad line objects are indicated by squares, while narrow line objects are indicated by circles.

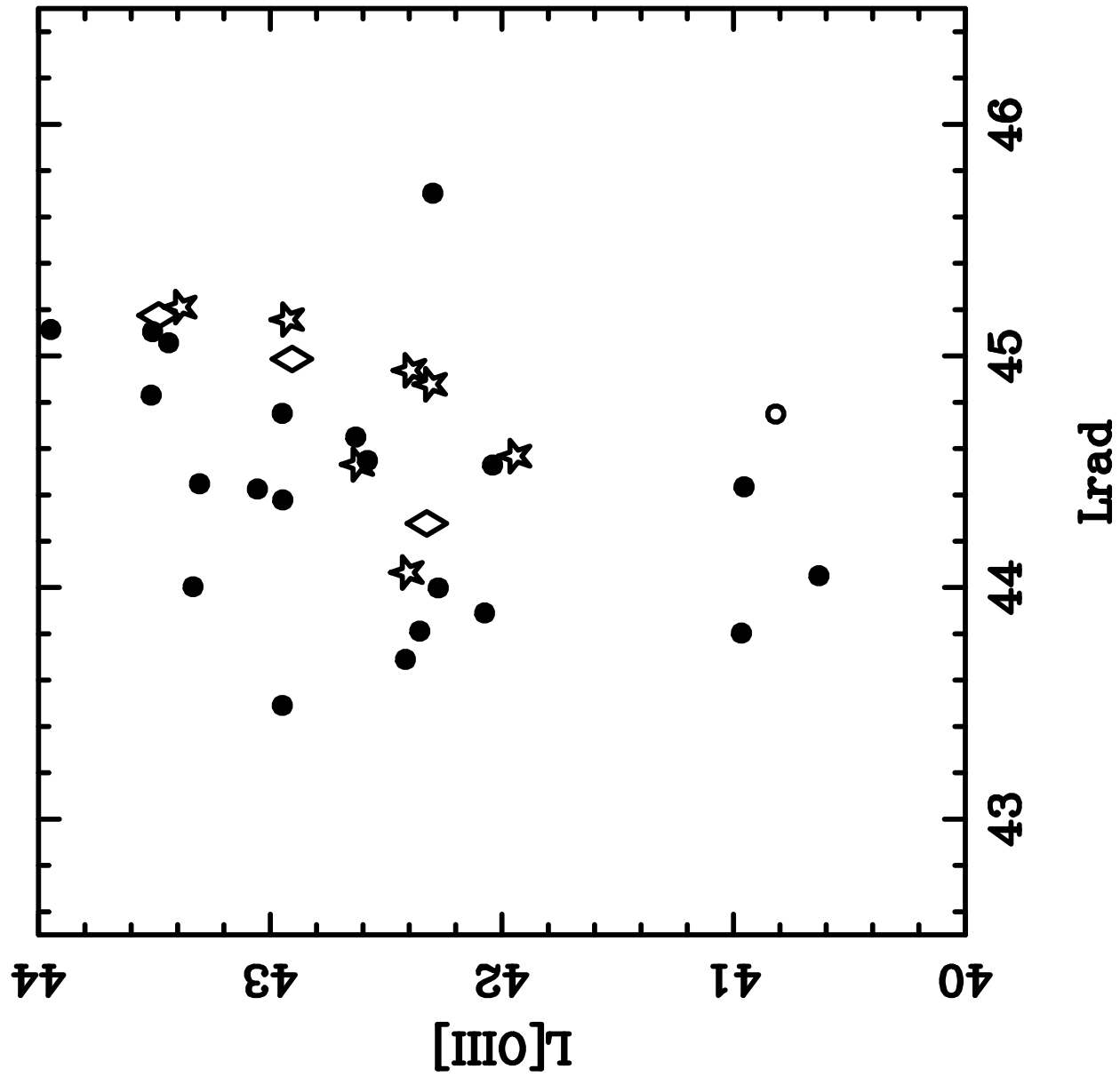
## Table captions.

**Table 1.** Basic data for the SSS sub-sample (see text for definition). The optical classifications (column 3) are explained in the text, while the radio classifications (column 4) are as follows: FRI — Fanaroff Riley Class I; FRII — Fanaroff Riley Class II; CSS — compact steep spectrum radio source ( $D < 15\text{kpc}$ ); and C/J — core-jet (uncertain classifications in brackets). The units of the total radio luminosities (column 6) and  $[\text{OIII}]\lambda 5007$  emission line luminosities (column 7) are  $\log(\text{erg s}^{-1})$ . The final two columns give, respectively, the  $[\text{OII}](3727)/[\text{OIII}](5007)$  and  $[\text{OIII}](5007)/\text{H}\beta$  diagnostic emission line ratios. Most of the emission line luminosities are based on the wide slit data presented in Tadhunter *et al.* (1993), but for cases in which the data in Tadhunter *et al.* (1993) are incomplete, we have used the deeper, but narrower slit, observations presented in Dickson (1997). All the spectral classifications of the sources (column 3) have been updated to take into account the new information in the deeper spectra (uncertain classifications in brackets). Note that, although 0347+05 is listed as a WLRG, it could also be classified as a BLRG since its spectrum shows broad permitted lines. The classification of 1932-46 as a BLRG is based on the high resolution optical spectra presented in Villar-Martin *et al.* (1997).

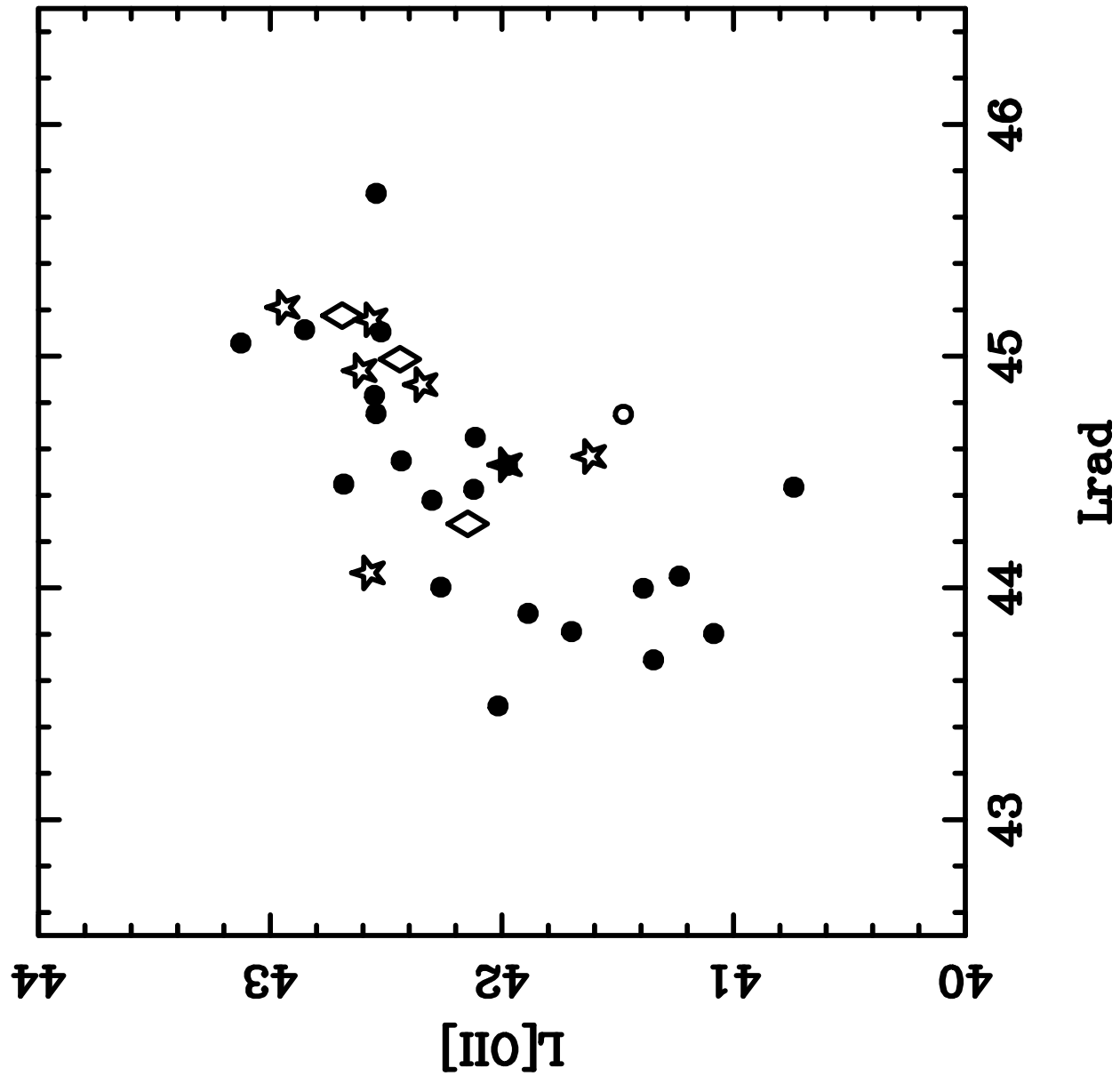
**Table 2.** Correlation analysis for the  $0.1 < z < 0.7$  SSS sub-sample. The first number given in each column is the Spearman’s  $\rho$  correlation coefficient, while the second number (in brackets) gives the significance level of the correlation (*i.e.* the percentage probability that the correlations could arise by chance). The analysis has been performed separately for the full  $0.1 < z < 0.7$  SSS sub-sample (column 2), for the  $0.1 < z < 0.7$  SSS sub-sample excluding the quasars (column 3), and for the  $0.1 < z < 0.7$  SSS sub-sample excluding quasars and WLRG (column 4).

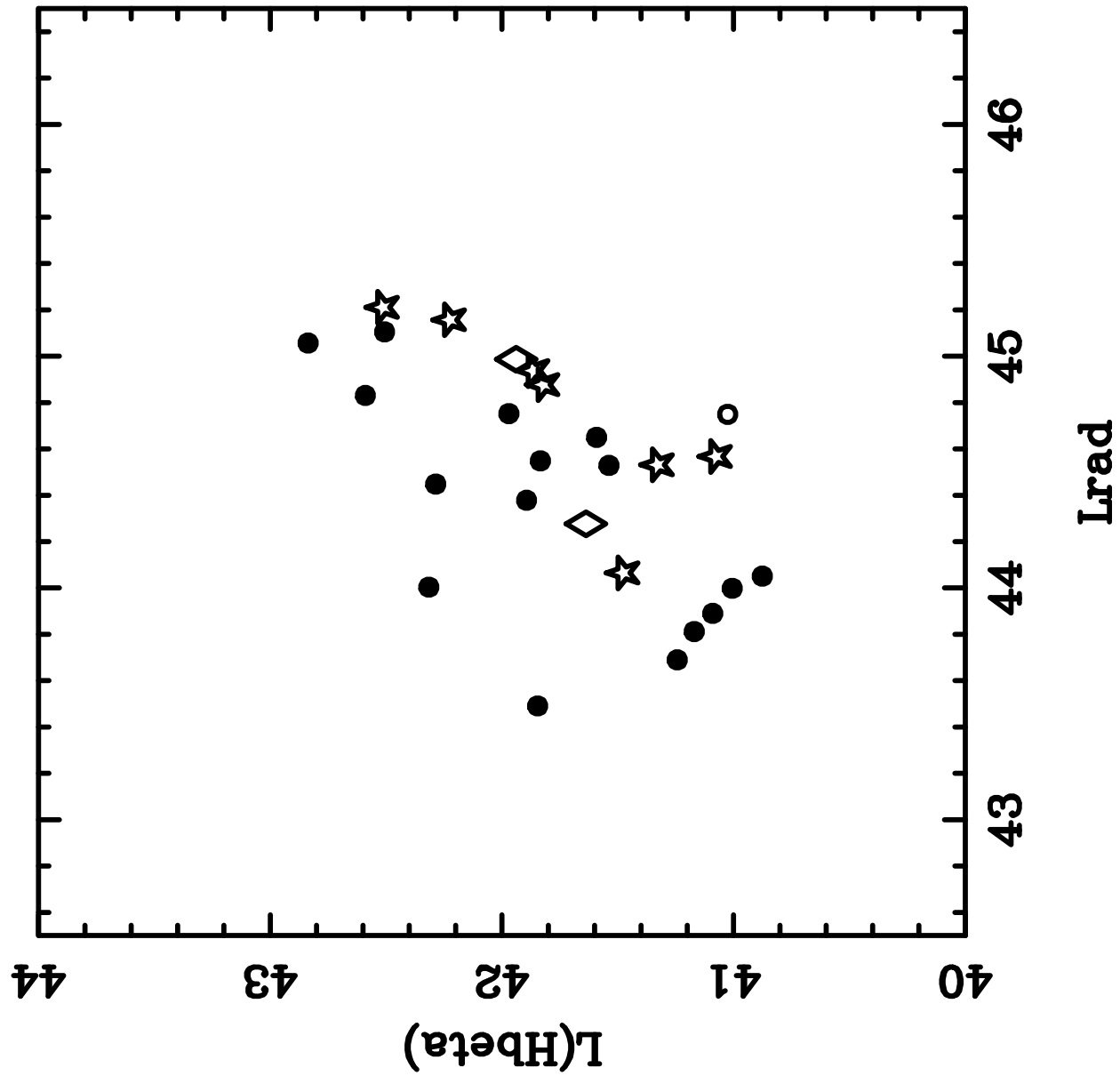
**Table 3.** Median ionization state ( $[\text{OII}](3727)/[\text{OIII}](5007)$ ), total radio luminosities, and  $[\text{OIII}]\lambda 5007$  emission line luminosities for the SSS subsample in different redshift ranges. Note that there is no evidence for a systematic increase in ionization state with redshift and radio power.

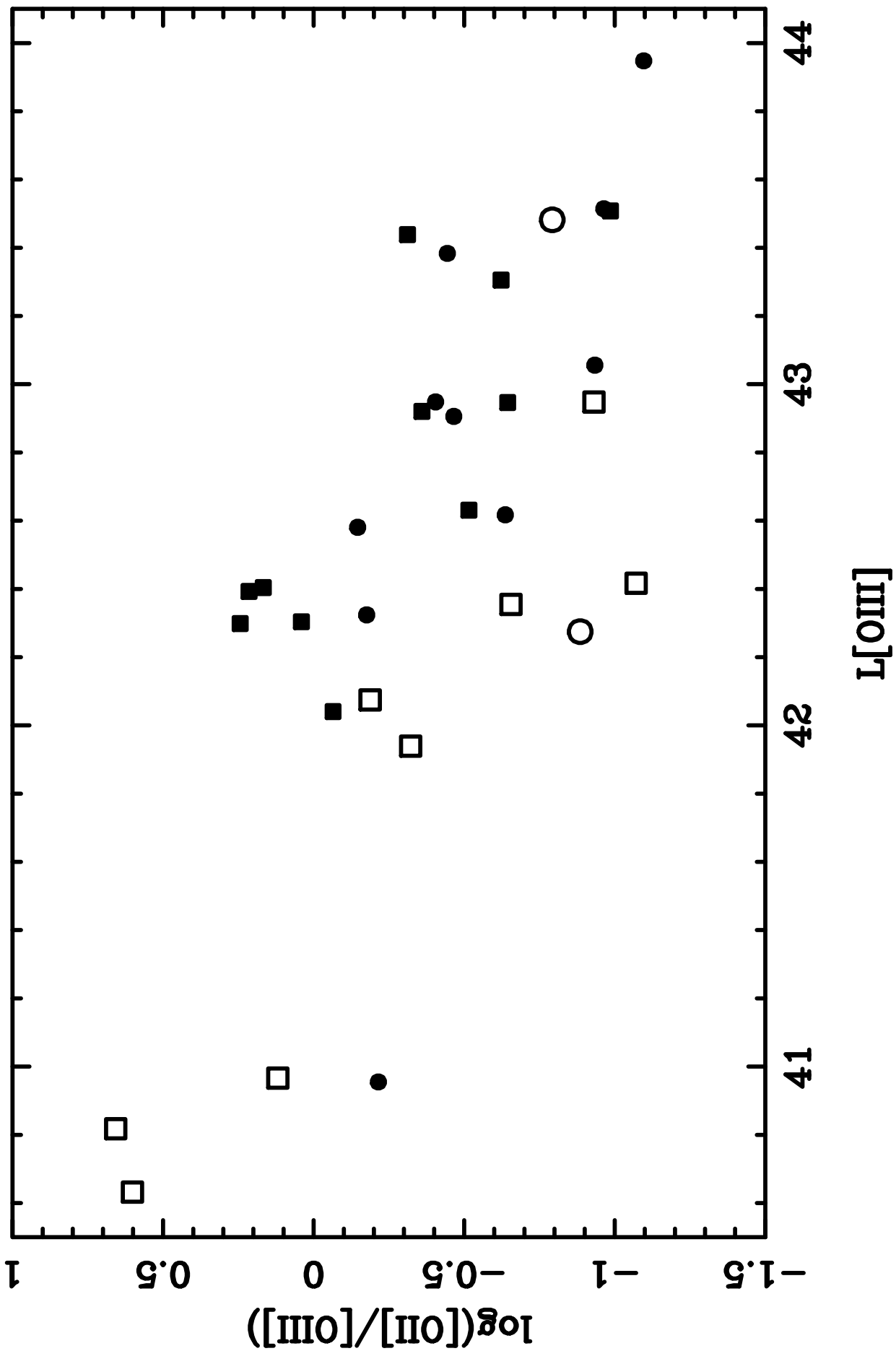


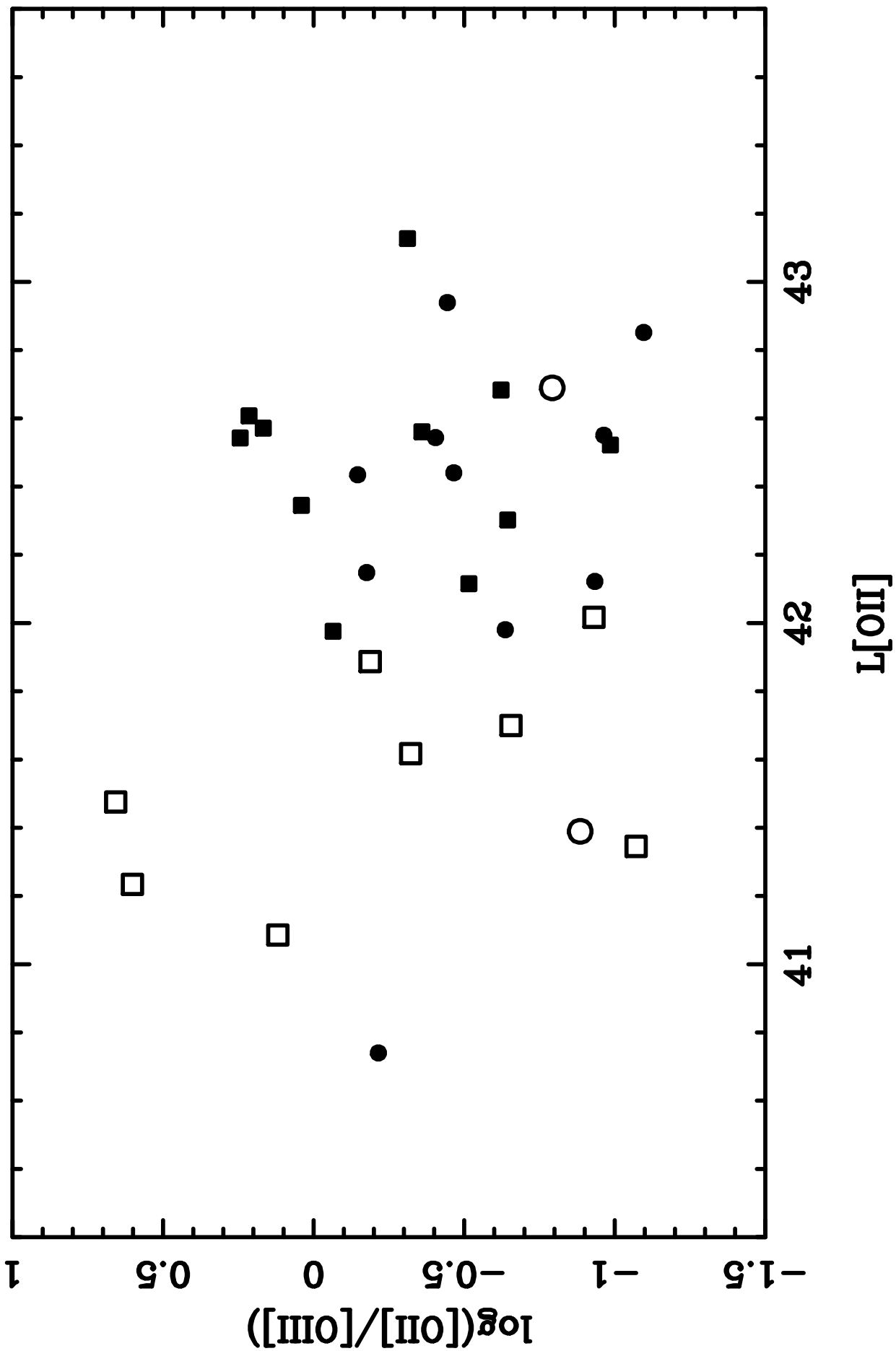


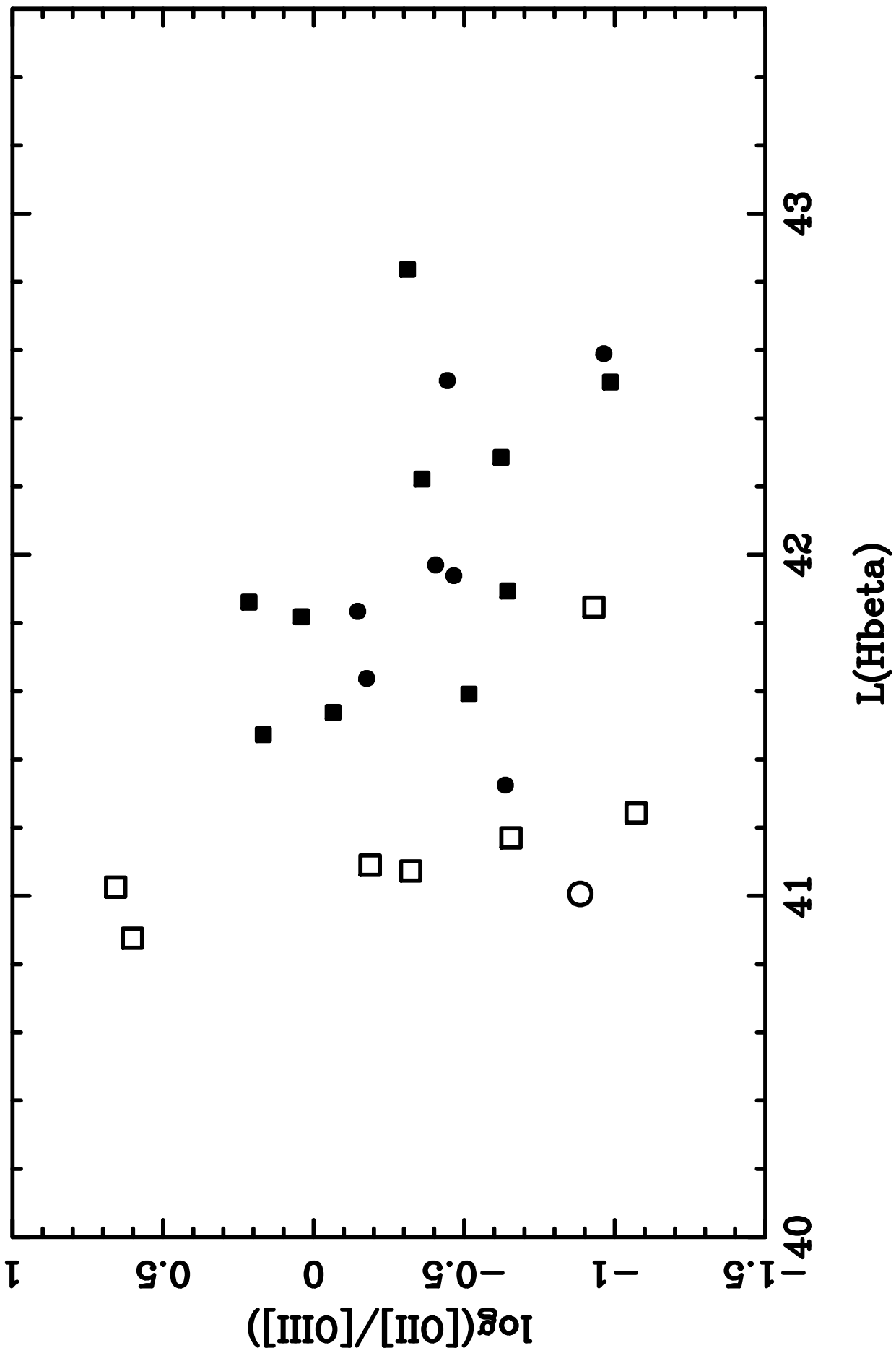


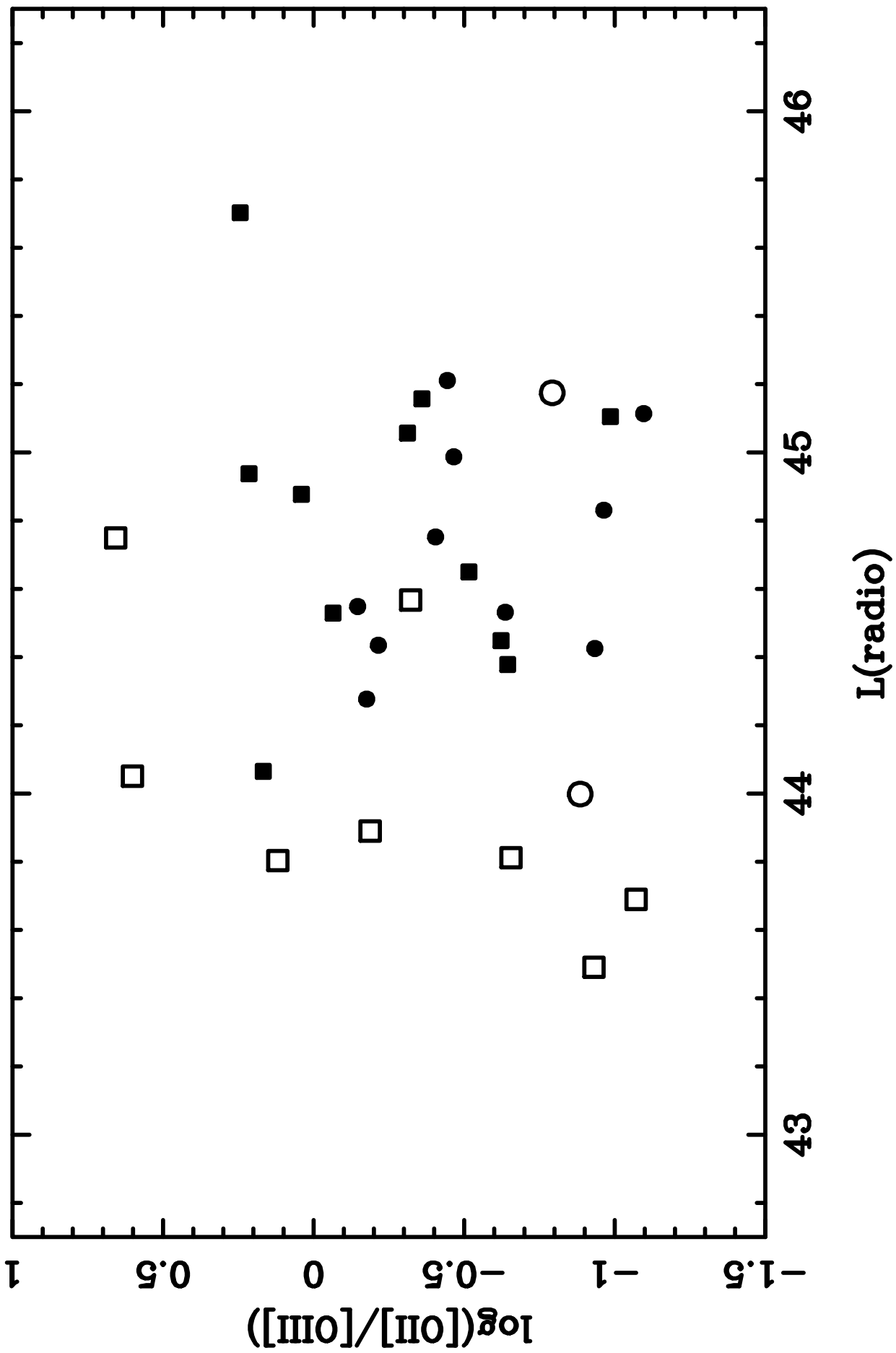


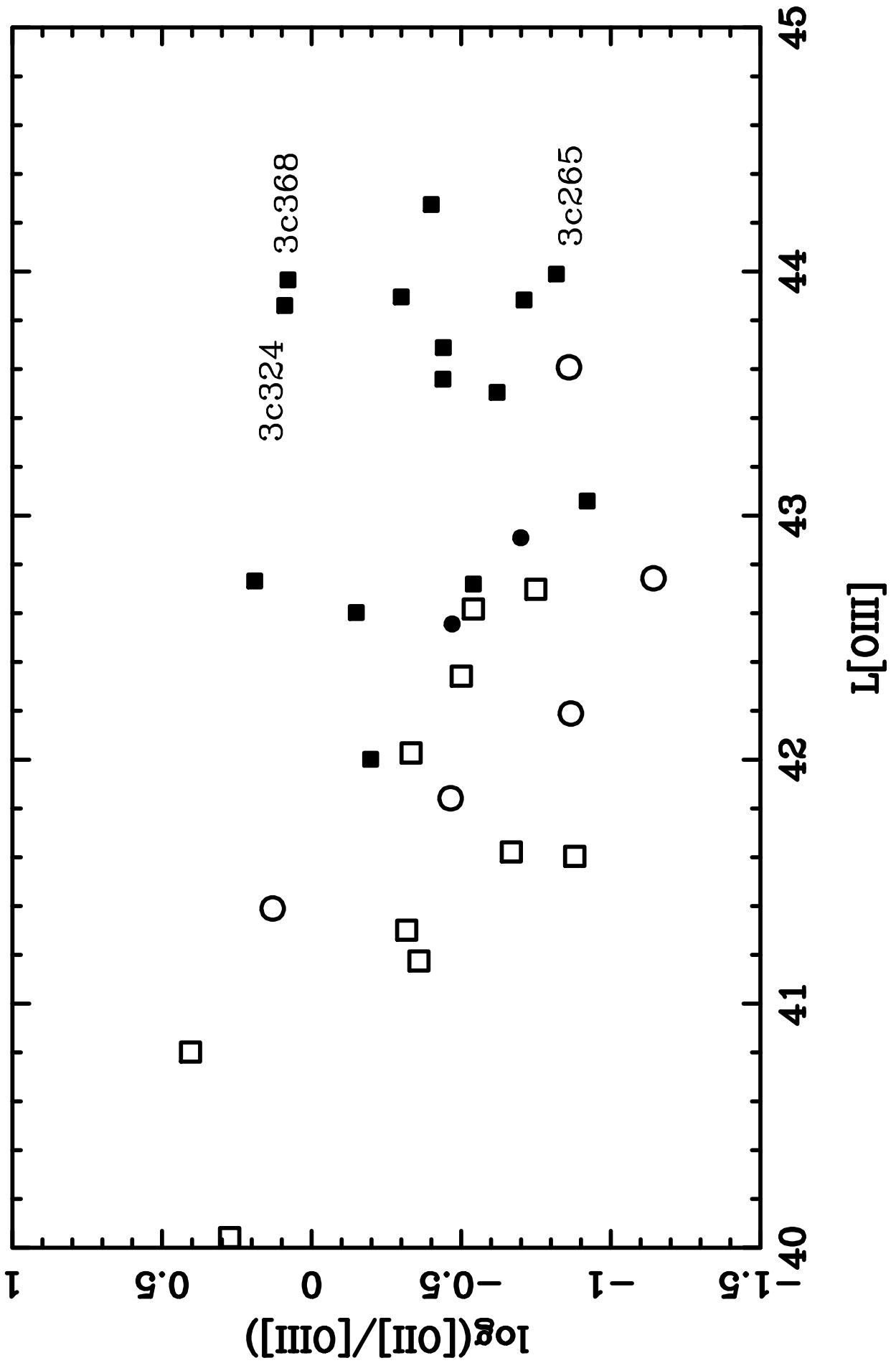


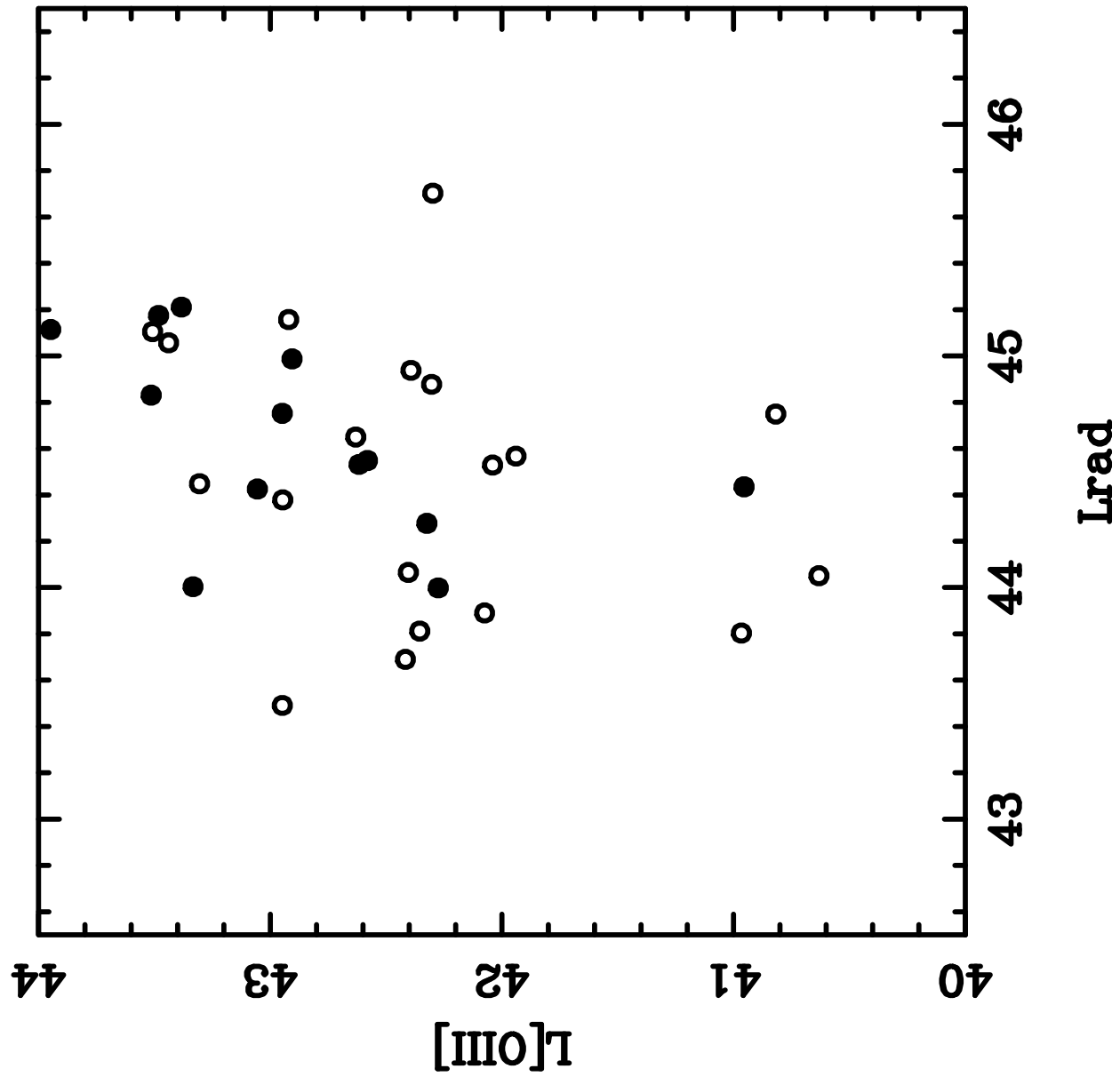




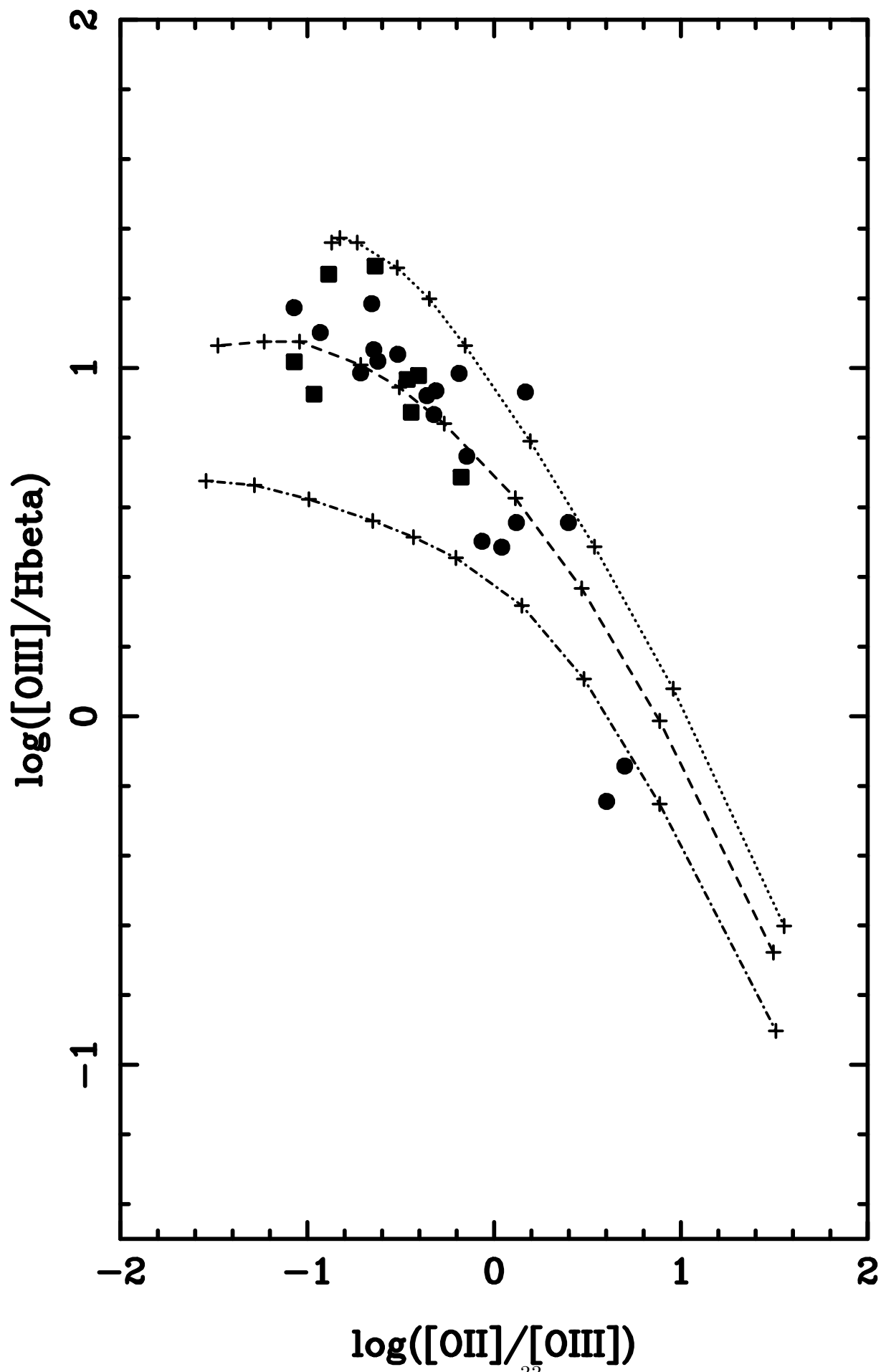












Object				z	$L_{rad}$	$L_{[OIII]}$	$[OIII]/[OII]$	$[OIII]/H_{\beta}$
0023–26		NLRG	CSS	0.322	44.88	42.30	0.91	3.06
0034–01		WLRG	FRII	0.073	43.07	40.76	—	3.69
0035–02	3C17	BLRG	(FRII)	0.220	44.28	42.32	1.50	4.86
0038+09	3C18	BLRG	FRII	0.188	44.00	42.27	7.68	18.58
0039–44		NLRG	FRII	0.346	44.45	43.31	4.19	10.46
0043–42		WLRG	FRII	0.116	43.80	40.97	0.76	—
0055–01	3C29	WLRG	FRI	0.045	42.83	40.20	—	1.65
0105–16	3C32	NLRG	FRII	0.400	44.65	42.63	3.28	10.95
0117–15	3C38	NLRG	FRII	0.565	45.06	43.44	2.05	4.00
0123–01	3C40	WLRG	FRII	0.018	41.95	<39.20	—	—
0131–36	NGC612	WLRG	FRII	0.030	42.84	40.03	—	3.14
0213–13	3C62	NLRG	FRII	0.147	43.81	42.35	4.52	15.30
0235–19		BLRG	FRII	0.620	45.10	43.51	9.68	10.03
0252–71		NLRG	CSS	0.566	45.16	42.92	2.29	5.00
0255+05	3C75	WLRG	FRI	0.023	42.19	<39.27	—	—
0305+03	3C78	WLRG	FRI	0.029	42.62	<39.48	—	—
0320–37	Fornax A	WLRG	FRI	0.005	42.52	<38.94	—	—
0325+02	3C88	WLRG	FRII	0.030	42.40	39.84	—	—
0347+05		BLRG	FRII	0.339	44.43	40.95	1.64	—
0349–27		NLRG	FRII	0.066	43.19	41.36	0.59	6.90
0404+03	3C105	NLRG	FRII	0.089	43.53	41.16	—	15.92
0409–75		NLRG	FRII	0.693	45.70	42.30	0.57	—
0428–53		WLRG	FRI	0.038	43.16	<39.22	—	—
0442–28		NLRG	FRII	0.147	43.89	42.07	1.54	9.65
0453–20		WLRG	FRI	0.035	42.54	<39.52	—	—
0518–45	Pictor A	BLRG	FRII	0.035	43.46	41.54	1.77	4.21
0521–36		BLRG	C/J	0.055	43.69	41.15	3.13	5.47
0625–53		WLRG	(FRII)	0.054	42.97	<39.67	—	—
0625–35		WLRG	FRI	0.055	42.97	<39.96	—	—
0806–10		NLRG	FRII	0.110	43.49	42.95	8.53	12.64
0859–25		NLRG	FRII	0.305	44.53	42.04	1.16	3.18
0915–11	Hydra A	WLRG	FRI	0.054	43.78	40.63	0.15	0.75
0945+07	3C227	BLRG	FRII	0.086	43.47	42.15	12.67	9.01
1136–13		Q	FRII	0.554	45.11	43.95	12.48	—
1151–34		Q	CSS	0.258	44.53	42.62	4.33	19.61
1216+06	3C270	WLRG	FRI	0.006	41.75	<38.56	—	—
1226+02	3C273	Q	C/J	0.158	45.17	43.48	—	—
1246–41	NGC4696	WLRG	FRI	0.009	41.20	<38.52	—	—
1251–12	3C278	WLRG	FRI	0.015	41.92	<39.06	—	—
1306–09		NLRG	CSS	0.464	44.94	42.39	0.61	3.40
1318–43	NGC5090	WLRG	FRI	0.011	41.62	<38.74	—	—
1333–33	IC4296	WLRG	FRI	0.013	41.96	<39.11	—	—
1355–41		Q	FRII	0.313	44.43	43.06	8.59	—

Object				z	$L_{rad}$	$L_{[OIII]}$	$[OIII]/[OII]$	$[OIII]/H_{\beta}$
1547-79		BLRG	FRII	0.483	44.83	43.51	9.20	8.41
1559+02	3C327	NLRG	FRII	0.104	43.69	42.42	11.78	14.90
1602+01	3C327.1	NLRG	FRII	0.462	44.75	42.95	2.54	9.51
1637-77		WLRG	FRII	0.041	42.83	40.73	1.06	9.61
1648+05	Hercules A	WLRG	FRI/FRII	0.154	44.75	40.82	0.22	0.62
1717-00	3C353	WLRG	FRII	0.031	43.46	39.69	—	0.92
1733-56		BLRG	FRII	0.098	43.42	41.97	1.39	5.72
1814-63		NLRG	CSS	0.063	43.42	40.81	—	—
1932-46		BLRG	FRII	0.231	44.55	42.58	1.40	5.58
1934-63		NLRG	CSS	0.183	44.57	41.94	2.10	7.35
1938-15		BLRG	FRII	0.452	44.99	42.91	2.92	9.27
1949+02	3C403	NLRG	FRII	0.059	43.12	41.91	8.41	20.10
1954-55		WLRG	FRI	0.060	43.05	<39.22	—	—
2058-28		WLRG	FRI	0.038	42.63	39.73	—	1.03
2104-25		WLRG	FRII	0.037	42.71	40.13	—	—
2135-14		Q	FRII	0.200	44.00	43.33	11.74	10.42
2135-20		BLRG	CSS	0.635	45.21	43.38	2.78	7.46
2152-69		BLRG	FRII	0.027	43.16	41.10	2.47	7.42
2211-17	3C444	WLRG	FRII	0.153	44.05	40.63	0.25	0.57
2221-02	3C445	BLRG	FRII	0.057	43.07	42.41	14.10	12.88
2250-41		NLRG	FRII	0.310	44.38	42.95	4.41	11.29
2314+03	3C459	NLRG	(CSS)	0.220	44.07	42.40	0.68	8.53
2356-61		NLRG	FRII	0.096	44.02	42.22	2.65	12.62

Correlation	Full SSD ( $z > 0.1$ )	No quasars	No quasars, no WLRG
$L_{[OIII]} \text{ vs } L_{radio}$	0.329( $\sim 5\%$ )	0.382( $\sim 2.5\%$ )	0.323( $\sim 5\%$ )
$L_{[OII]} \text{ vs } L_{radio}$	0.606( $< 0.1\%$ )	0.656( $< 0.1\%$ )	0.667( $< 0.1\%$ )
$L_{radio} \text{ vs } z$	0.742( $< 0.1\%$ )	0.907( $< 0.1\%$ )	0.938( $< 0.1\%$ )
$L_{[OIII]} \text{ vs } z$	0.488( $\sim 0.5\%$ )	0.551( $\sim 0.5\%$ )	0.450( $\sim 1\%$ )
$L_{[OII]} \text{ vs } z$	0.698( $< 0.1\%$ )	0.735( $< 0.1\%$ )	0.778( $< 0.1\%$ )
$L_{[OIII]} \text{ vs } L_{[OII]}$	0.740( $< 0.1\%$ )	0.728( $< 0.1\%$ )	0.471( $\sim 1\%$ )
$[OII]/[OIII] \text{ vs } L_{radio}$	-0.08( $> 10\%$ )	-0.134( $> 10\%$ )	-0.299( $\sim 10\%$ )
$[OII]/[OIII] \text{ vs } L_{[OIII]}$	0.710( $< 0.1\%$ )	0.641( $< 0.1\%$ )	0.464( $\sim 1\%$ )
$[OII]/[OIII] \text{ vs } L_{[OII]}$	0.122( $> 10\%$ )	-0.084( $> 10\%$ )	-0.294( $\sim 10\%$ )

Redshift range	N	Median [OII]/[OIII]	Median $L_{radio}$	Median $L_{[OIII]}$
0.1 – 0.2	10	0.30	43.94	42.17
0.2 – 0.3	5	0.67	44.28	42.58
0.3 – 0.4	6	0.34	44.44	42.62
0.4 – 0.5	5	0.34	44.89	42.63
0.5 – 0.6	3	0.44	45.11	43.44
0.6 – 0.7	3	0.36	45.21	43.38